Title: CDC20B is required for deuterosome-mediated centriole production in multiciliated cells

Authors: Diego R. Revinski[1†], Laure-Emmanuelle Zaragosi[2†], Camille Boutin[1†], Sandra Ruiz-Garcia[2], Marie Deprez[2], Virginie Thomé[1], Olivier Rosnet[1], Anne-Sophie Gay[2], Olivier Mercey[2], Agnès Paquet[2], Nicolas Pons[2], Gilles Ponzio[2], Brice Marcet[2*], Laurent Kodjabachian[1*], Pascal Barbry[2*]

Affiliations:

[1] Aix Marseille Univ, CNRS, IBDM, Marseille, France

[2] Université Côte d'Azur, CNRS, IPMC, Sophia-Antipolis, France.

[†] These authors contributed equally

[*]Correspondence to: marcet@ipmc.cnrs.fr; laurent.kodjabachian@univ-amu.fr; barbry@ipmc.cnrs.fr

Keywords: multiciliated cell, centriole, deuterosome, motile cilia, CDC20B, Separase, PLK1, cell cycle, *Xenopus*, mouse, human

Abstract: Multiciliated cells (MCCs) harbour dozens to hundreds of motile cilia, which beat in a synchronized and directional manner, thus generating hydrodynamic forces important in animal physiology. In vertebrates, MCC differentiation critically depends on the synthesis and release of numerous centrioles by specialized structures called deuterosomes. Little is known about the composition, organization and regulation of deuterosomes. Here, single-cell RNA sequencing reveals that human deuterosome-stage MCCs are characterized by the expression of many cell cycle-related genes. We further investigated the uncharacterized vertebrate-specific *cell division cycle 20B* (*CDC20B*) gene, the host gene of microRNA-449abc. We show that the CDC20B protein associates to deuterosomes and is required for the release of centrioles and the subsequent production of cilia in mouse and *Xenopus* MCCs. CDC20B interacts with PLK1, which has been shown to coordinate centriole disengagement with the protease Separase in mitotic cells. Strikingly, over-expression of Separase rescued centriole disengagement and cilia production in CDC20B-deficient MCCs. This work reveals the shaping of a new biological function, deuterosome-mediated centriole production in vertebrate MCCs, by adaptation of canonical and recently evolved cell cycle-related molecules.

Multiciliated cells (MCCs) are present throughout metazoan evolution and serve functions ranging from locomotion of marine larvae and flatworms, to brain homeostasis, mucociliary clearance of pathogens and transportation of oocytes in vertebrates[1-3]. The formation of MCCs requires the production of numerous motile cilia through a complex process called multiciliogenesis[2, 3]. The transcriptional control of multiciliogenesis has been decrypted to a large extent, through studies in *Xenopus* and mouse[2]. Seating at the top of the cascade, the Geminin-related factors GemC1[4-7] and Multicilin[8, 9] (MCIDAS in mammals) are both necessary and sufficient to initiate MCC differentiation. GemC1 and Multicilin in complex with E2F transcription factors have been reported to activate the expression of Myb, FoxJ1, Rfx2 and

Rfx3, which collectively regulate the expression of a large body of effectors required for the formation of multiple motile cilia[4, 5, 8-11]. Recently, defective multiciliogenesis caused by mutations in MCIDAS and Cyclin O (CCNO) has been associated with congenital respiratory and fertility syndromes in human[12, 13].

Each cilium sits atop a modified centriole, called a basal body (BB). After they exit from the cell cycle, maturing MCCs face the challenge of producing dozens to hundreds of centrioles in a limited time window. In vertebrate MCCs, bulk centriole biogenesis is mostly achieved through an acentriolar structure named the deuterosome, although canonical amplification from parental centrioles also occurs[1-3]. The deuterosome was first described in early electron microscopy studies of various multiciliated tissues including the mammalian lung[14] and oviduct[15, 16], the avian trachea[17], and the *Xenopus* tadpole epidermis and trachea[18]. In mammalian MCCs, the deuterosome was described as a spherical mass of fibers organized into an inner dense region and an outer, more delicate, corona[16]. In *Xenopus*, deuterosomes were initially named procentriole organizers and were reported as dense amorphous masses[18]. Recent studies have revealed that deuterosome-mediated centriole synthesis mobilizes key components of the centriole-dependent duplication pathway of the cell cycle, including CEP152, PLK4 and SAS6[19-21]. However, the deuterosome itself differs from the centriole and may contain specific components. The identification of one such component, called DEUP1 for Deuterosome assembly protein 1, opened the possibility to investigate the deuterosome at the molecular level[21]. In mouse tracheal ependymal cells, DEUP1 was detected in the core of the deuterosome[21]. DEUP1, also known as CCDC67, is a conserved vertebrate paralogue of CEP63, itself known for its importance in initiation of centriole duplication during the cell cycle[21, 22]. Consistently, DEUP1 was shown to be essential for centriole multiplication in mouse and *Xenopus* MCCs[21]. Both CEP63 and DEUP1 interact with CEP152, an event essential for centriole duplication and multiplication in cycling cells and MCCs, respectively[21, 22]. Once

centriole multiplication is over, neo-synthesized centrioles must disengage from deuterosomes and parental centrioles, convert into BBs and migrate apically to dock at the plasma membrane to initiate cilium elongation.

In this study, we aimed at better understanding deuterosome biology. We found that the gene *CDC20B* was specifically expressed in maturing MCCs during the phase of centriole multiplication. We established the corresponding CDC20B protein as an essential regulator of centriole-deuterosome disengagement. This work illustrates well the strong functional relationships that exist between centriole release from deuterosomes and centriole disengagement in mitotic cells. It also posits CDC20B as a new component of a "multiciliary locus" that contains several gene products, either proteins, such as MCIDAS, CCNO or CDC20B itself, or microRNAs, such as miR-449abc, which are all actively involved into multiciliogenesis.

Results

To identify new regulators of centriole multiplication, we analyzed the transcriptome of human airway epithelial cells (HAECs) at the differentiation stage corresponding to active centriole multiplication[23] at the single-cell level (Fig. 1a). Gene expression data from 1663 cells was projected on a 2D space by *t*-distributed Stochastic Neighbor Embedding (tSNE) (Fig. 1b). We identified a small group of 37 cells corresponding to maturing MCCs engaged in deuterosome-mediated centriole amplification, as revealed by the specific expression of *MCIDAS*[8], *MYB*[24], and *DEUP1*[21] (Fig. 1c,d and Supplementary Fig. 1). This subpopulation was characterized by the expression of known effectors of centriole synthesis, such as *PLK4*, *STIL*, *CEP152*, *SASS6*, but also of cell cycle regulators, such as *CDK1*, *CCNB1*, *CDC20*, *SGOL2* and *NEK2* (Fig. 1d, Supplementary Fig. 1 and Supplementary Table 1). We reasoned that uncharacterized cell cycle-related genes that are specific to this subpopulation could encode new components of the

deuterosome-dependent centriole amplification pathway. A particularly interesting candidate in this category was *CDC20B* (Fig. 1d), which is related to the cell cycle regulators *CDC20* and *FZR1*[25] (Supplementary Fig. 2a). First, the *CDC20B* gene is present in the vertebrate genomic locus that also contains the key MCC regulators *MCIDAS*[8] and *CCNO*[13]. Co-expression of *CDC20B*, *MCIDAS* and *CCNO* throughout HAEC differentiation was indeed observed in an independent RNA sequencing study, performed on a bulk population of HAECs (Supplementary Fig. 2b). These results fit well with the observation that the promoter of human *CDC20B* was strongly activated by the MCIDAS partners E2F1 and E2F4 (Supplementary Fig. 2c), as also shown in *Xenopus* by others[9] (Supplementary Fig. 2d). Second, the *CDC20B* gene bears in its second intron the miR-449 microRNAs, which were shown to contribute to MCC differentiation[23, 26-30]. Finally, in *Xenopus* epidermal MCCs, *cdc20b* transcripts were specifically detected during the phase of centriole amplification (Supplementary Fig. 2e-m). This first set of data pointed out the specific and conserved expression pattern of *CDC20B* in immature MCCs. In the rest of this study, we analyzed the putative role of CDC20B in deuterosome-mediated centriole multiplication,.

We first conducted a series of immunofluorescence analyses to gain a better understanding of deuterosome organization in mouse ependymal and *Xenopus* epidermal MCCs as models. In whole-mounts of mouse ependymal walls, mature deuterosomes revealed by DEUP1 staining appeared as circular structures around a lumen (Fig. 2a). We noticed that DEUP1 also stained fibers emanating from the core into the corona. Nascent centrioles revealed by the marker FOP were organized around the DEUP1-positive core ring. STED super-resolution microscopy helped to better appreciate the regular organization of individual FOP-positive procentrioles (Fig. 2b). Proximity labeling assays have revealed that when ectopically expressed in centrosomes CCDC67/DEUP1 is found close to Pericentrin (PCNT) and γ-tubulin, two main components of the pericentriolar material (PCM)[31]. Interestingly, we found that PCNT was

120 present in the deuterosome corona (Fig. 2a), and STED microscopy further revealed that PCNT
121 formed fibers around growing procentrioles (Fig. 2b). γ-tubulin staining was detected in the
122 DEUP1-positive deuterosome core, as well as in the corona (Fig. 2a). STED microscopy
123 indicated that PCNT and γ-tubulin stained distinct interwoven fibers in the deuterosome corona.
124 Next, we stained immature *Xenopus* epidermal MCCs with γ-Tubulin and Centrin to reveal
125 centriole amplification platforms. These platforms displayed irregular shapes and sizes (Fig.
126 2c), in agreement with early electron microscopy studies[18]. Expression of low amounts of GFP-
127 Deup1 in MCCs induced by Multicilin confirmed that active deuterosomes are embedded in γ-
128 Tubulin-positive masses (Fig. 2d). Overall, this analysis is consistent with early ultrastructural
129 studies, as the deuterosome core and corona can be distinguished by the presence of DEUP1
130 and PCNT, respectively. Moreover, γ-tubulin is a conserved marker of centriole amplification
131 platforms in vertebrate MCCs. By analogy to the organization of the centrosome, we propose
132 to coin the term perideuterosomal material (PDM) to describe the corona, as this region may
133 prove important for deuterosome function.
134 We then analyzed the subcellular localization of CDC20B protein in deuterosome-stage mouse
135 and *Xenopus* MCCs. In immature mouse tracheal MCCs, double immunofluorescence revealed
136 the association of CDC20B to DEUP1-positive deuterosomes (Fig. 3a). We noticed that
137 CDC20B tended to associate primarily to large DEUP1 foci. As deuterosomes grow as they
138 mature[21], this suggests that CDC20B may penetrate into the deuterosomal environment at a late
139 stage of the centriole multiplication process. The same observation was made when comparing
140 CDC20B staining in the region of immature and mature deuterosomes of mouse ependymal
141 MCCs (Fig. 3b). As double DEUP1/CDC20B staining could not be performed on these cells,
142 we analyzed CDC20B distribution relative to FOP-positive procentrioles. In early
143 deuterosome-stage MCCs, CDC20B was expressed at low levels and FOP staining was mostly
144 concentrated in a large amorphous cloud (Fig. 3b). In such cells, no CDC20B staining was

detected in association to FOP-positive procentrioles growing around deuterosomes. In contrast, in mature deuterosome-stage MCCs, CDC20B was enriched in the innermost part of the PDM, probably very close to the deuterosome core (Fig. 3b). Further evidence was provided with a custom-made polyclonal antibody (Supplementary Fig. 3b,c) used to analyze Cdc20b protein distribution in *Xenopus* epidermal MCCs. Here also, Cdc20b was found associated to Deup1-positive deuterosomes actively engaged in centriole synthesis (Fig. 3c). We finally analyzed the distribution of CDC20B in mature MCCs. As previously reported, the CDC20B protein was detected near BBs[23], but also in cilia of fully differentiated human airway MCCs (Supplementary Fig. 4a-c). This was confirmed by proximity ligation assays that revealed a tight association of CDC20B with Centrin2 and acetylated α-Tubulin, in BBs and cilia, respectively (Supplementary Fig. 4d-f). Fluorescent immunostaining also revealed the presence of Cdc20b in the vicinity of BBs in *Xenopus* epidermal MCCs (Supplementary Fig. 4g-i). In contrast, no cilia staining was observed in these cells. We conclude that in three distinct types of MCCs in two distant vertebrate species, CDC20B is tightly associated to mature deuterosomes. We next investigated whether it may control their function.

For that purpose, *Cdc20b* was knocked down in mouse ependymal MCCs, through post-natal brain electroporation of three distinct shRNAs. One of them, sh274, which targets the junction between exons 3 and 4, and can therefore only interact with mature mRNA, was useful to rule out possible interference with the production of miR-449 molecules from the *Cdc20b* pre-mRNA (Supplementary Fig. 5a). Five days after electroporation, all three shRNAs significantly reduced the expression of CDC20B in deuterosome-stage MCCs (Fig. 4c), but did not alter MCC identity as revealed by FOXJ1 expression (Fig. 4a,b,d). Centriole production by deuterosomes was analyzed by FOP/DEUP1 double staining nine days after electroporation. At this stage, control MCCs had nearly all released their centrioles and disassembled their deuterosomes (Fig. 4e,g). In sharp contrast, *Cdc20b* shRNAs caused a significant increase in

the number of defective MCCs that displayed centrioles still engaged on deuterosomes (Fig. 4f,g). Fifteen days after electroporation, a majority of CDC20B-deficient MCCs still showed a severely reduced number of released centrioles, and consequently lacked cilia (Fig. 4h-k).

Cdc20b was also knocked down in *Xenopus* epidermal MCCs, through injection of two independent morpholino antisense oligonucleotides targeting either the ATG (Mo ATG), or the exon 1/intron 1 junction (Mo Spl) (Supplementary Fig. 5b). The efficiency of Mo ATG was verified through fluorescence extinction of co-injected Cdc20b-Venus (Supplementary Fig. 5c). RT-PCR confirmed that Mo Spl caused intron 1 retention (Supplementary Fig. 5d), which was expected to introduce a premature stop codon, and to produce a Cdc20b protein lacking 96% of its amino-acids, likely to undergo unfolded protein response-mediated degradation. Thus, both morpholinos were expected to generate severe loss of Cdc20b function. Consistent with this interpretation, both morpholinos strongly reduced Cdc20b immunostaining in deuterosome-stage MCCs (Supplementary Fig. 5e). We verified that neither morpholinos caused *p53* transcript up-regulation (Supplementary Fig. 5f), a non-specific response to morpholinos that is sometimes detected in zebrafish embryos[32]. Importantly, whole-mount *in situ* hybridization indicated that miR-449 expression was not perturbed in the presence of either morpholino (Supplementary Fig. 5g). We found that *cdc20b* knockdown did not interfere with acquisition of the MCC fate (Supplementary Fig. 6a-e), but severely impaired multiciliogenesis, as revealed by immunofluorescence and electron microscopy (Fig. 5a-i). This defect stemmed from a dramatic reduction in the number of centrioles, and poor docking at the plasma membrane (Fig. 5g-o and Supplementary Fig. 6f-k). Importantly, centrioles and cilia were rescued in Mo Spl MCCs by co-injection of *cdc20b*, *venus-cdc20b* or *cdc20b-venus* mRNAs (Fig. 5j-o and Supplementary Fig. 6f-k). In normal condition, *Xenopus* epidermal MCCs arise in the inner mesenchymal layer and intercalate into the outer epithelial layer, while the process of centriole amplification is underway[33]. To rule out secondary defects due to poor radial

intercalation, we assessed the consequences of *cdc20b* knockdown in MCCs induced in the outer layer by Multicilin overexpression[8]. Like in natural MCCs, Cdc20b proved to be essential for the production of centrioles and cilia in response to Multicilin activity (Supplementary Fig. 7a-g). We also noted that the apical actin network that normally surrounds BBs was not maintained in absence of Cdc20b, although this defect could be secondary to the absence of centrioles (Supplementary Fig. 7d-g). Centrioles in Cdc20b morphant cells often formed clusters, suggesting that disengagement from deuterosomes could have failed (Fig. 5l,m). To better assess this process we injected GFP-Deup1 in Multicilin-induced MCCs and stained centrioles with Centrin. In mature control MCCs, deuterosomes were disassembled, centrioles were converted into BBs, had docked and initiated cilium growth (Fig. 5p,s). In contrast, both morpholinos caused a dramatic increase in the number of defective MCCs, which were devoid of cilia and displayed centrioles still engaged on deuterosomes (Fig. 5q-u). Altogether our functional assays in mouse and *Xenopus* indicate that CDC20B is required for centriole disengagement from deuterosomes and subsequent ciliogenesis in MCCs. We next investigated the molecular mechanism of action of CDC20B underlying its role in centriole release.

In mitotic cells, centriole disengagement is necessary to license centriole duplication in the following cell cycle[34]. This process is known to depend on the coordinated activities of the mitotic kinase PLK1 and the protease Separase[35]. One proposed mechanism involves the phosphorylation of PCNT by PLK1, which induces its cleavage by Separase, thereby allowing centriole disengagement through disassembly of the PCM[36, 37] (Fig. 7h). Separase is known to be activated by the degradation of its inhibitor Securin, which is triggered by the Anaphase Promoting Complex (APC/C) upon binding to CDC20[25]. *PLK1*, *Separase* (*ESPL1*), *Securin* (*PTTG1*), *CDC20* and *PCNT* were all found to be expressed in human deuterosome-stage MCCs (Fig. 1d and Supplementary Fig. 1). We have shown above that PCNT is present in the PDM and a recent study revealed the presence of CDC20 and the APC/C component APC3 in

mouse ependymal MCCs at the stage of centriole disengagement[38]. Based on this large body of information, we hypothesized that centriole-deuterosome disengagement involves the coordinated activities of PLK1 and Separase, and that CDC20B would be involved in this scenario. *CDC20B* encodes a protein of about 519 amino-acids largely distributed across the vertebrate phylum[23]. In its C-terminal half, CDC20B contains seven well conserved WD40 repeats, predicted to form a β-propeller, showing 49% and 37% identity to CDC20 and FZR1 repeats, respectively (Supplementary Fig. 2a). However, CDC20B lacks canonical APC/C binding domains (Supplementary Fig. 2a). Using mass spectrometry on immunoprecipitated protein complexes from transfected HEK cells, we could identify multiple APC/C components interacting with CDC20 but not with CDC20B (Supplementary Table 2). We conclude that CDC20B is probably incapable of activating APC/C. Interestingly, an unbiased interactome study reported association of CDC20B with PLK1[39]. Using reciprocal co-immunoprecipitation assays in HEK transfected cells, we confirmed that CDC20B and PLK1 could be found in the same complex (Fig. 6a). This suggested that CDC20B could cooperate with PLK1 to trigger centriole disengagement. Consistent with this hypothesis, we found that PLK1 was enriched in the PDM of mature deuterosomes in mouse ependymal MCCs (Fig. 6d), in agreement with a recent report[38]. Another interesting partner of CDC20B identified in a second unbiased interactome study[40] was SPAG5 (Astrin), which was reported to control timely activation of Separase during the cell cycle[41, 42]. Using the same strategy as above, we could detect CDC20B and SPAG5 in the same complex (Fig. 6b). As SPAG5 was found associated to DEUP1 in a proximity labeling assay[31], we assessed its localization in deuterosomes. Strikingly, SPAG5 was detectable in mature deuterosomes of mouse ependymal MCCs, with a clear enrichment in the deuterosome core (Fig. 6d). Finally, reciprocal co-immunoprecipitations revealed that CDC20B and DEUP1 were detected in the same complex when co-expressed in HEK cells (Fig. 6c). Consistent with this result, we observed that RFP-Cdc20b was recruited around spherical

Deup1-GFP structures positive for γ-Tubulin and Centrin in *Xenopus* epidermal MCCs (Supplementary Fig. 7h-m). This series of experiments suggested that CDC20B could participate in the assembly of a protein complex in mature deuterosomes, required to coordinate the activities of PLK1 and Separase for centriole disengagement. As Separase is the last effector in this scenario, we tested whether over-expressing human Separase in *Xenopus cdc20b* morphant MCCs could rescue centriole disengagement. In support to our hypothesis, over-expression of wild-type, but not protease-dead Separase, efficiently rescued centriole disengagement and cilia formation in *cdc20b* morphant MCCs (Fig. 7a-g and Supplementary Fig. 7n-s). Separase could also rescue multiciliogenesis in Multicilin-induced MCCs injected with *cdc20b* Mos (Supplementary Fig. 7t-z). We conclude that CDC20B is involved in Separase-mediated release of mature centrioles from deuterosomes in vertebrate MCCs (Fig. 7h).

Discussion

In this study, we report for the first time the essential and conserved role of CDC20B in vertebrate multiciliogenesis. Our data suggest that the presence of CDC20B in the perideuterosomal region is necessary to allow Separase-dependent proteolysis leading to centriole disengagement. Our findings are consistent with a recent report showing that centriole disengagement in murine ependymal MCCs involves the activities of PLK1 and APC/C[38]. How are CDC20B and Separase activities integrated? The simple scenario of a CDC20-like function of CDC20B is very unlikely as it does not appear to bind APC/C (Supplementary Table 2). CDC20 was detected in cultured murine ependymal MCCs during the phase of centriole disengagement[38], and FZR1 genetic ablation was reported to cause reduced production of centrioles and cilia in the same cells[43]. APC/C is therefore likely activated in maturing MCCs by its classical activators, CDC20 and/or FZR1, leading to Separase activation through

degradation of its inhibitor Securin. In that context, we propose that additional factors linked directly or indirectly to CDC20B may contribute to activation of Separase. It was shown that SPAG5 inhibits or activates Separase depending on its status of phosphorylation[41, 42]. As the phosphorylation status of SPAG5 was shown to be controlled by PLK1[44], our data suggest that the CDC20B/PLK1/SPAG5 complex could control the timing of Separase activation locally in deuterosomes. It is therefore possible that multiple modes of activation of Separase may act in parallel to trigger the release of neo-synthesized centrioles in maturing MCCs. Alternatively, different pathways may be used in distinct species, or in distinct types of MCCs. An important question for future studies regards the identity of PLK1 and Separase substrates involved in centriole disengagement. Work on mitotic cells[36, 37] and our own analysis suggest that PCNT may represent a prime target. Another potentially relevant candidate could be DEUP1 itself as it is clear that deuterosomes are disassembled after the release of centrioles. In that respect, it is interesting to note the presence of multiple PLK1 consensus phosphorylation sites in human, mouse and *Xenopus* DEUP1.

In this study, we have introduced the notion of perideuterosomal material, in analogy to the pericentriolar material. It is striking that the two main components of the PCM, PCNT and γ-Tubulin, are also present in the PDM, which begs the question whether additional PCM proteins may be present in the PDM. The PDM may constitute a platform to sustain procentriole growth, through the concentration and delivery of elementary parts. It could also play a mechanical role to hold in place the growing procentrioles. Future work should evaluate deuterosome-mediated centriole synthesis in absence of major PDM components.

We found that beyond its association to deuterosomes during the phase of centriole amplification, CDC20B was also associated to BBs and cilia in fully differentiated mammalian MCCs. This dual localization is consistent with failed ciliogenesis upon CDC20B knockdown in mouse ependymal MCCs. However, while we could detect Cdc20b near BBs of mature

MCCs in *Xenopus*, we found no evidence of its presence in cilia. Furthermore, cilia were rescued by Separase overexpression in Cdc20b morphant MCCs. This suggests that Cdc20b is not required for ciliogenesis in this species, although it could potentially contribute to cilium structure and/or function. Thus, refined temporal and spatial control of CDC20B inhibition will be needed to study its function beyond centriole synthesis.

This and previous studies[23, 26-28] establish that the miR-449 cluster and its host gene *CDC20B* are commonly involved in multiciliogenesis. Consistent with its early expression, it was suggested that miR-449 controls cell cycle exit and entry into differentiation of MCCs[23, 27, 30]. This study reveals that CDC20B itself is involved in the production of centrioles, the first key step of the multiciliogenesis process. From that perspective, the nested organization of miR-449 and *CDC20B* in vertebrate genomes, which allows their coordinated expression, appears crucial for successful multiciliogenesis.

It is also noteworthy to point out the location of this gene in a genomic locus where congenital mutations in MCIDAS and CCNO were recently shown to cause a newly-recognized MCC-specific disease, called Reduced Generation of Multiple motile Cilia (RGMC). RGMC is characterized by severe chronic lung infections and increased risk of infertility[12, 13]. Its location in the same genetic locus as MCIDAS and CCNO makes CDC20B a putative candidate for RGMC. By extension, new deuterosome-stage specific genes uncovered by scRNA-seq in this study also represent potential candidates for additional RGMC mutations.

Previous works have established the involvement of the centriole duplication machinery active in S-phase of the cell cycle, during centriole multiplication of vertebrate post-mitotic MCCs[19-21]. Our study further reveals a striking analogy between centriole disengagement from deuterosomes in MCCs, and centriole disengagement that occurs during the M/G1 transition of the cell cycle (Fig. 7g). Thus, it appears that centriole production in MCCs recapitulates the key steps of the centriole duplication cycle[34]. However, the cell cycle machinery must adapt to the

acentriolar deuterosome to massively produce centrioles. Such adaptation appears to involve physical and functional interactions between canonical cell cycle molecules, such as CEP152 and PLK1, and recently evolved cell cycle-related deuterosomal molecules, such as DEUP1[21] and CDC20B. It remains to examine whether additional deuterosomal cell cycle-related molecules have emerged in the vertebrate phylum to sustain massive centriole production.

In conclusion, this work illustrates how coordination between ancestral and recently evolved cell cycle-related molecules can give rise to a new differentiation mechanism in vertebrates.

References

1. Meunier, A. & Azimzadeh, J. Multiciliated Cells in Animals. *Cold Spring Harb Perspect Biol* **8** (2016).
2. Spassky, N. & Meunier, A. The development and functions of multiciliated epithelia. *Nat Rev Mol Cell Biol* **18**, 423-436 (2017).
3. Brooks, E.R. & Wallingford, J.B. Multiciliated cells. *Curr Biol* **24**, R973-982 (2014).
4. Kyrousi, C. *et al.* Mcidas and GemC1 are key regulators for the generation of multiciliated ependymal cells in the adult neurogenic niche. *Development* **142**, 3661-3674 (2015).
5. Arbi, M. *et al.* GemC1 controls multiciliogenesis in the airway epithelium. *EMBO Rep* **17**, 400-413 (2016).
6. Terre, B. *et al.* GEMC1 is a critical regulator of multiciliated cell differentiation. *EMBO J* **35**, 942-960 (2016).
7. Zhou, F. *et al.* Gmnc Is a Master Regulator of the Multiciliated Cell Differentiation Program. *Curr Biol* **25**, 3267-3273 (2015).
8. Stubbs, J.L., Vladar, E.K., Axelrod, J.D. & Kintner, C. Multicilin promotes centriole assembly and ciliogenesis during multiciliate cell differentiation. *Nat Cell Biol* **14**, 140-147 (2012).
9. Ma, L., Quigley, I., Omran, H. & Kintner, C. Multicilin drives centriole biogenesis via E2f proteins. *Genes Dev* **28**, 1461-1471 (2014).
10. Quigley, I.K. & Kintner, C. Rfx2 Stabilizes Foxj1 Binding at Chromatin Loops to Enable Multiciliated Cell Gene Expression. *PLoS Genet* **13**, e1006538 (2017).
11. Chung, M.I. *et al.* RFX2 is broadly required for ciliogenesis during vertebrate development. *Dev Biol* **363**, 155-165 (2012).
12. Boon, M. *et al.* MCIDAS mutations result in a mucociliary clearance disorder with reduced generation of multiple motile cilia. *Nat Commun* **5**, 4418 (2014).
13. Wallmeier, J. *et al.* Mutations in CCNO result in congenital mucociliary clearance disorder with reduced generation of multiple motile cilia. *Nat Genet* **46**, 646-651 (2014).
14. Sorokin, S.P. Reconstructions of centriole formation and ciliogenesis in mammalian lungs. *J Cell Sci* **3**, 207-230 (1968).
15. Dirksen, E.R. Centriole morphogenesis in developing ciliated epithelium of the mouse oviduct. *J Cell Biol* **51**, 286-302 (1971).
16. Anderson, R.G. & Brenner, R.M. The formation of basal bodies (centrioles) in the Rhesus monkey oviduct. *J Cell Biol* **50**, 10-34 (1971).

17. Kalnins, V.I. & Porter, K.R. Centriole replication during ciliogenesis in the chick tracheal epithelium. *Z Zellforsch Mikrosk Anat* **100**, 1-30 (1969).
18. Steinman, R.M. An electron microscopic study of ciliogenesis in developing epidermis and trachea in the embryo of Xenopus laevis. *Am J Anat* **122**, 19-55 (1968).
19. Al Jord, A. *et al.* Centriole amplification by mother and daughter centrioles differs in multiciliated cells. *Nature* **516**, 104-107 (2014).
20. Klos Dehring, D.A. *et al.* Deuterosome-mediated centriole biogenesis. *Dev Cell* **27**, 103-112 (2013).
21. Zhao, H. *et al.* The Cep63 paralogue Deup1 enables massive de novo centriole biogenesis for vertebrate multiciliogenesis. *Nat Cell Biol* **15**, 1434-1444 (2013).
22. Sir, J.H. *et al.* A primary microcephaly protein complex forms a ring around parental centrioles. *Nat Genet* **43**, 1147-1153 (2011).
23. Marcet, B. *et al.* Control of vertebrate multiciliogenesis by miR-449 through direct repression of the Delta/Notch pathway. *Nat Cell Biol* **13**, 693-699 (2011).
24. Tan, F.E. *et al.* Myb promotes centriole amplification and later steps of the multiciliogenesis program. *Development* **140**, 4277-4286 (2013).
25. Yu, H. Cdc20: a WD40 activator for a cell cycle degradation machine. *Mol Cell* **27**, 3-16 (2007).
26. Song, R. *et al.* miR-34/449 miRNAs are required for motile ciliogenesis by repressing cp110. *Nature* **510**, 115-120 (2014).
27. Otto, T. *et al.* Cell cycle-targeting microRNAs promote differentiation by enforcing cell-cycle exit. *Proc Natl Acad Sci U S A* **114**, 10660-10665 (2017).
28. Wu, J. *et al.* Two miRNA clusters, miR-34b/c and miR-449, are essential for normal brain development, motile ciliogenesis, and spermatogenesis. *Proc Natl Acad Sci U S A* **111**, E2851-2857 (2014).
29. Chevalier, B. *et al.* miR-34/449 control apical actin network formation during multiciliogenesis through small GTPase pathways. *Nat Commun* **6**, 8386 (2015).
30. Mercey, O. *et al.* Characterizing isomiR variants within the microRNA-34/449 family. *FEBS Lett* **591**, 693-705 (2017).
31. Firat-Karalar, E.N., Rauniyar, N., Yates, J.R., 3rd & Stearns, T. Proximity interactions among centrosome components identify regulators of centriole duplication. *Curr Biol* **24**, 664-670 (2014).
32. Robu, M.E. *et al.* p53 activation by knockdown technologies. *PLoS Genet* **3**, e78 (2007).
33. Werner, M.E. *et al.* Radial intercalation is regulated by the Par complex and the microtubule-stabilizing protein CLAMP/Spef1. *J Cell Biol* **206**, 367-376 (2014).
34. Firat-Karalar, E.N. & Stearns, T. The centriole duplication cycle. *Philos Trans R Soc Lond B Biol Sci* **369** (2014).
35. Tsou, M.F. *et al.* Polo kinase and separase regulate the mitotic licensing of centriole duplication in human cells. *Dev Cell* **17**, 344-354 (2009).
36. Kim, J., Lee, K. & Rhee, K. PLK1 regulation of PCNT cleavage ensures fidelity of centriole separation during mitotic exit. *Nat Commun* **6**, 10076 (2015).
37. Matsuo, K. *et al.* Kendrin is a novel substrate for separase involved in the licensing of centriole duplication. *Curr Biol* **22**, 915-921 (2012).
38. Al Jord, A. *et al.* Calibrated mitotic oscillator drives motile ciliogenesis. *Science* **358**, 803-806 (2017).
39. Huttlin, E.L. *et al.* The BioPlex Network: A Systematic Exploration of the Human Interactome. *Cell* **162**, 425-440 (2015).
40. Rual, J.F. *et al.* Towards a proteome-scale map of the human protein-protein interaction network. *Nature* **437**, 1173-1178 (2005).

411 41. Thein, K.H., Kleylein-Sohn, J., Nigg, E.A. & Gruneberg, U. Astrin is required for the
412 maintenance of sister chromatid cohesion and centrosome integrity. *J Cell Biol* **178**, 345-354
413 (2007).
414 42. Chiu, S.C. *et al.* The mitosis-regulating and protein-protein interaction activities of
415 astrin are controlled by aurora-A-induced phosphorylation. *Am J Physiol Cell Physiol* **307**,
416 C466-478 (2014).
417 43. Eguren, M. *et al.* The APC/C cofactor Cdh1 prevents replicative stress and p53-
418 dependent cell death in neural progenitors. *Nat Commun* **4**, 2880 (2013).
419 44. Chung, H.J., Park, J.E., Lee, N.S., Kim, H. & Jang, C.Y. Phosphorylation of Astrin
420 Regulates Its Kinetochore Function. *J Biol Chem* **291**, 17579-17592 (2016).
421 45. Qiu, X. *et al.* Single-cell mRNA quantification and differential analysis with Census.
422 *Nat Methods* **14**, 309-315 (2017).
423 46. Macosko, E.Z. *et al.* Highly Parallel Genome-wide Expression Profiling of Individual
424 Cells Using Nanoliter Droplets. *Cell* **161**, 1202-1214 (2015).
425 47. Kim, D. *et al.* TopHat2: accurate alignment of transcriptomes in the presence of
426 insertions, deletions and gene fusions. *Genome Biol* **14**, R36 (2013).
427 48. Anders, S., Pyl, P.T. & Huber, W. HTSeq--a Python framework to work with high-
428 throughput sequencing data. *Bioinformatics* **31**, 166-169 (2015).
429 49. Love, M.I., Huber, W. & Anders, S. Moderated estimation of fold change and dispersion
430 for RNA-seq data with DESeq2. *Genome Biol* **15**, 550 (2014).
431 50. Langmead, B. & Salzberg, S.L. Fast gapped-read alignment with Bowtie 2. *Nat Methods*
432 **9**, 357-359 (2012).
433 51. Heinz, S. *et al.* Simple combinations of lineage-determining transcription factors prime
434 cis-regulatory elements required for macrophage and B cell identities. *Mol Cell* **38**, 576-589
435 (2010).
436 52. Boutin, C. *et al.* A dual role for planar cell polarity genes in ciliated cells. *Proc Natl*
437 *Acad Sci U S A* **111**, E3129-3138 (2014).
438 53. Boutin, C. *et al.* NeuroD1 induces terminal neuronal differentiation in olfactory
439 neurogenesis. *Proc Natl Acad Sci U S A* **107**, 1201-1206 (2010).
440 54. Boutin, C., Diestel, S., Desoeuvre, A., Tiveron, M.C. & Cremer, H. Efficient in vivo
441 electroporation of the postnatal rodent forebrain. *PLoS One* **3**, e1883 (2008).
442 55. You, Y. & Brody, S.L. Culture and differentiation of mouse tracheal epithelial cells.
443 *Methods Mol Biol* **945**, 123-143 (2013).
444 56. Marchal, L., Luxardi, G., Thome, V. & Kodjabachian, L. BMP inhibition initiates neural
445 induction via FGF signaling and Zic genes. *Proc Natl Acad Sci U S A* **106**, 17437-17442 (2009).
446 57. Castillo-Briceno, P. & Kodjabachian, L. Xenopus embryonic epidermis as a mucociliary
447 cellular ecosystem to assess the effect of sex hormones in a non-reproductive context. *Front*
448 *Zool* **11**, 9 (2014).
449 58. Deblandre, G.A., Wettstein, D.A., Koyano-Nakagawa, N. & Kintner, C. A two-step
450 mechanism generates the spacing pattern of the ciliated cells in the skin of Xenopus embryos.
451 *Development* **126**, 4715-4728 (1999).
452
453

454 **Acknowledgements**

455 We are grateful to Chris Kintner, Marc Kirschner, Olaf Stemmann, Reinhard Köster, Xavier

456 Morin and Xueliang Zhu for reagents. Imaging in IBDM was performed on PiCSL-FBI core

457 facility, supported by the French National Research Agency through the program "Investments
458 for the Future" (France-BioImaging, ANR-10-INBS-04). Sequencing at UCAGenomiX
459 (IPMC), a partner of the National Infrastructure France Génomique, was supported by
460 Commissariat aux Grands Investissements (ANR-10-INBS-09-03, ANR-10-INBS-09-02) and
461 Canceropôle PACA. The authors thank Florian Roguet for *Xenopus* care, and Nathalie Garin
462 from Leica Microsystems GmbH for technical advice on STED microscopy. We are grateful to
463 Rainer Waldmann, Kévin Lebrigand, Virginie Magnone and Nicolas Nottet for fruitful
464 discussions on single cell RNA sequencing, and Delphine Debayle for help with mass
465 spectrometry experiments. We thank Julien Royet and Harold Cremer for insightful comments
466 on the manuscript. This project was funded by grants from ANR (ANR-11-BSV2-021-02,
467 ANR-13-BSV4-0013, ANR-15-CE13-0003), FRM (DEQ20141231765, DEQ20130326464),
468 Fondation ARC (PJA 20161204865, PJA 20161204542), the labex Signalife (ANR-11-LABX-
469 0028-01), the association Vaincre la Mucoviscidose (RF20140501158, RF20120600738,
470 RF20150501288), and the Chan Zuckerberg Initiative (Silicon Valley Fundation, 2017-175159
471 -5022). OM, CB and DRR were supported by fellowships from Ligue Nationale contre le Cancer
472 (OM and CB), and Fondation ARC (DRR).

473

474 **Author contributions**

475 PB, BM and LK designed and supervised the study, and obtained funding. LEZ, SRG, OM
476 performed and analyzed human and mouse airway cells experiments. DRR and VT performed
477 and analyzed *Xenopus* experiments. CB performed and analyzed all experiments on mouse
478 ependymal MCCs and contributed to the description of *Xenopus* deuterosomes. OR
479 characterized CDC20B antibodies. MD and AP performed the bioinformatic analysis. NP
480 carried out scRNAseq experiments. ASG performed mass spectrometry analyses. GP designed
481 and performed CDC20B interaction studies. All authors were involved in data interpretation.

482 DRR, LEZ and CB designed the figures. LK drafted the original manuscript. DRR, LEZ, CB,

483 BM, PB and LK edited the manuscript.

484

485 **Competing financial interests**

486 The authors declare no competing financial interests.

487

488 **Figures and legends**

489

490

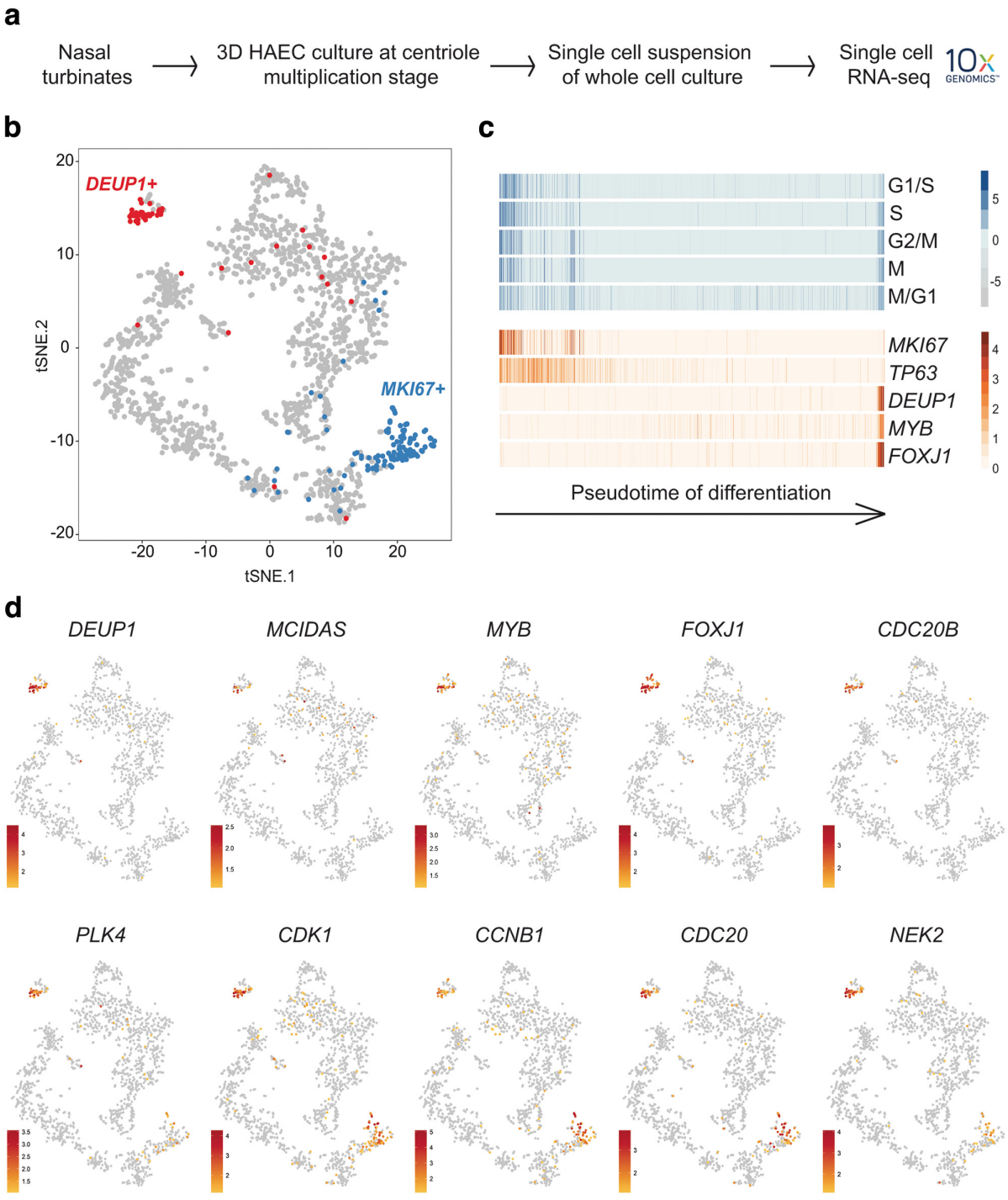

Figure 1: Single-cell RNA-seq analysis reveals *CDC20B* as a novel specific marker of deuterosomal stage MCCs, and enrichment of cell cycle-related genes in this cell population.

(**a**) Experimental design of the scRNA-seq experiment. (**b**) tSNE plot. Each point is a projection of a unique cell on a 2D space generated by the tSNE algorithm. Blue dots represent *MKI67*-

497 positive proliferating cells, and red dots represent *DEUP1*-positive cells corresponding to
498 maturing MCCs at deuterosome stage. (**c**) Cell cycle-related gene set expression in HAECs
499 measured by scRNA-seq. Cells were ordered along a pseudotime axis, defined with the
500 Monocle2 package. Phase specific scores are displayed in the top heatmap. Expression of
501 selected genes is displayed in the bottom heatmap. (**d**) tSNEs plots for a selection of genes
502 specifically enriched in deuterosome-stage cells. Note that *CDC20B* exhibits the most specific
503 expression among deuterosome marker genes.
504

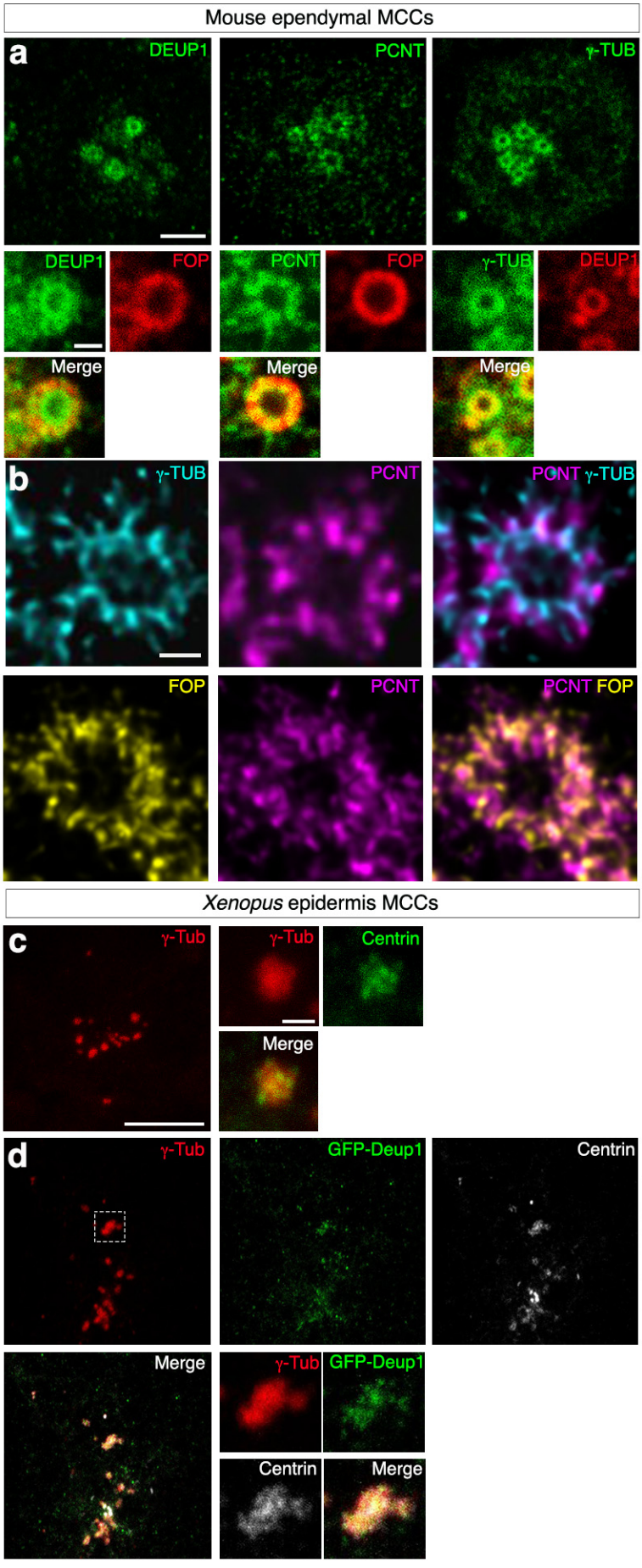

505

Figure 2: Composition and organization of vertebrate deuterosomes

(**a-b**) Maturing mouse ependymal MCCs were immunostained as indicated, pictures were taken with confocal (**a**) or STED (**b**) microscope. (**a**) DEUP1 stains the deuterosome core (ring) and a close fibrous area that defines the perideuterosomal region. The centriolar marker FOP reveals procentrioles arranged in a circle around the deuterosome. Pericentrin (PCNT) is enriched in the perideuterosomal region. γ-Tubulin (γ-TUB) stains the core as well as the periphery of the deuterosome. (**b**) STED pictures showing the organization of FOP, PCNT and γ-TUB in the perideuterosomal region. (**c**) *Xenopus* embryos were immunostained for γ-Tubulin (γ-Tub) and Centrin and high-magnification pictures of immature epidermal MCCs were taken. In these cells, Centrin-positive procentrioles grow around γ-Tubulin positive structures. (**d**) *Xenopus* embryos were injected with *Multicilin-hGR* and *GFP-Deup1* mRNAs, treated with dexamethasone at gastrula st11 to induce Multicilin activity, and immunostained at neurula st18 for γ-Tubulin, GFP and Centrin. Scale bars: 5µm (**a**, top), 500nm (**a**, bottom), 500nm (**b**), 10µm (**c**, **d**, large view), 1µm (**c**, **d**, high magnification).

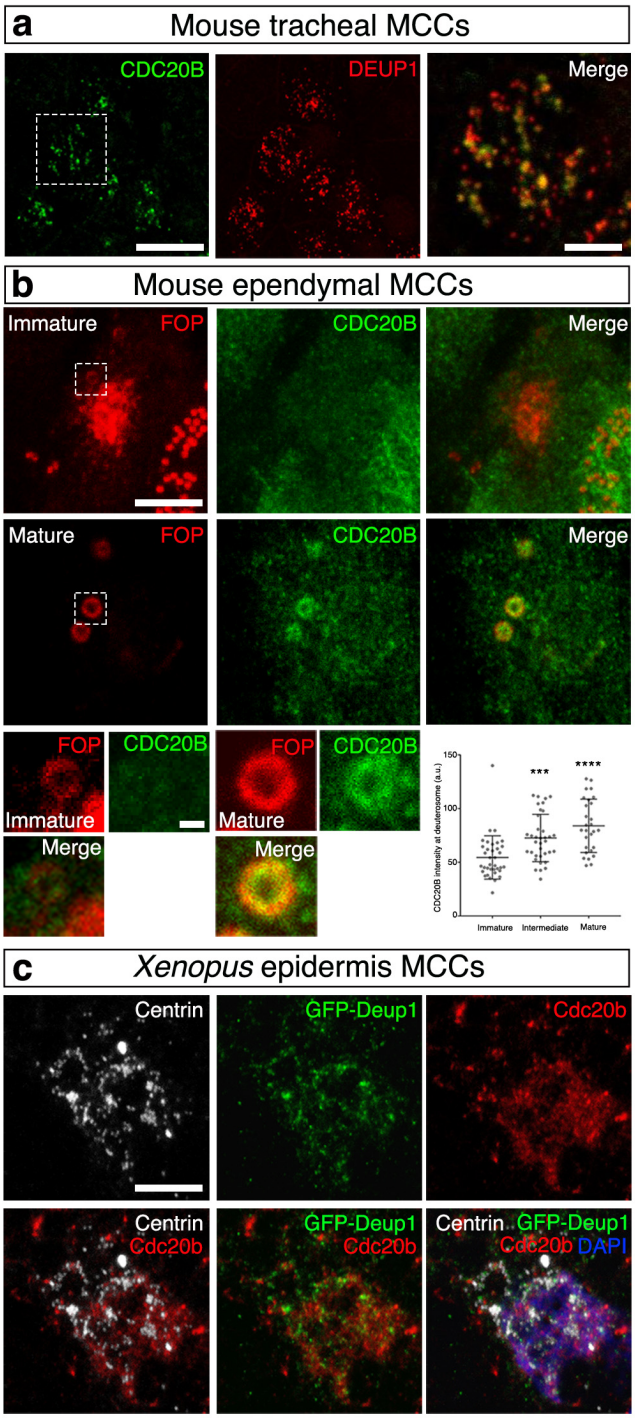

Figure 3: CDC20B is a component of vertebrate deuterosomes

(**a**) Double immunofluorescence was performed on mouse tracheal MCCs after 3 days of culture in air-liquid interface. Low magnification confocal panels show coincident CDC20B and DEUP1 staining in several individual MCCs. High magnification on a single MCC reveals the prominent association of CDC20B to deuterosomes marked by DEUP1. (**b**) Mouse

ependymal MCCs were immunostained as indicated, and high magnification confocal pictures of cells with immature and mature deuterosomal figures were taken. In these cells, centrioles revealed by FOP form a ring around deuterosomes. CDC20B staining forms a ring inside the ring of FOP-positive procentrioles indicating that CDC20B is tightly associated to deuterosomes. Note that the CDC20B signal associated to deuterosome increased with their maturation (high-magnification pictures quantified in the graph). (**c**) *Xenopus* embryos were injected with *GFP-Deup1* mRNA and immunostained at neurula st18 as indicated. Scale bars: 5µm (**a**, **b**, large view), 1.5µm (**a**, high magnification), 500nm (**b**, high magnification), 10µm (**c**).

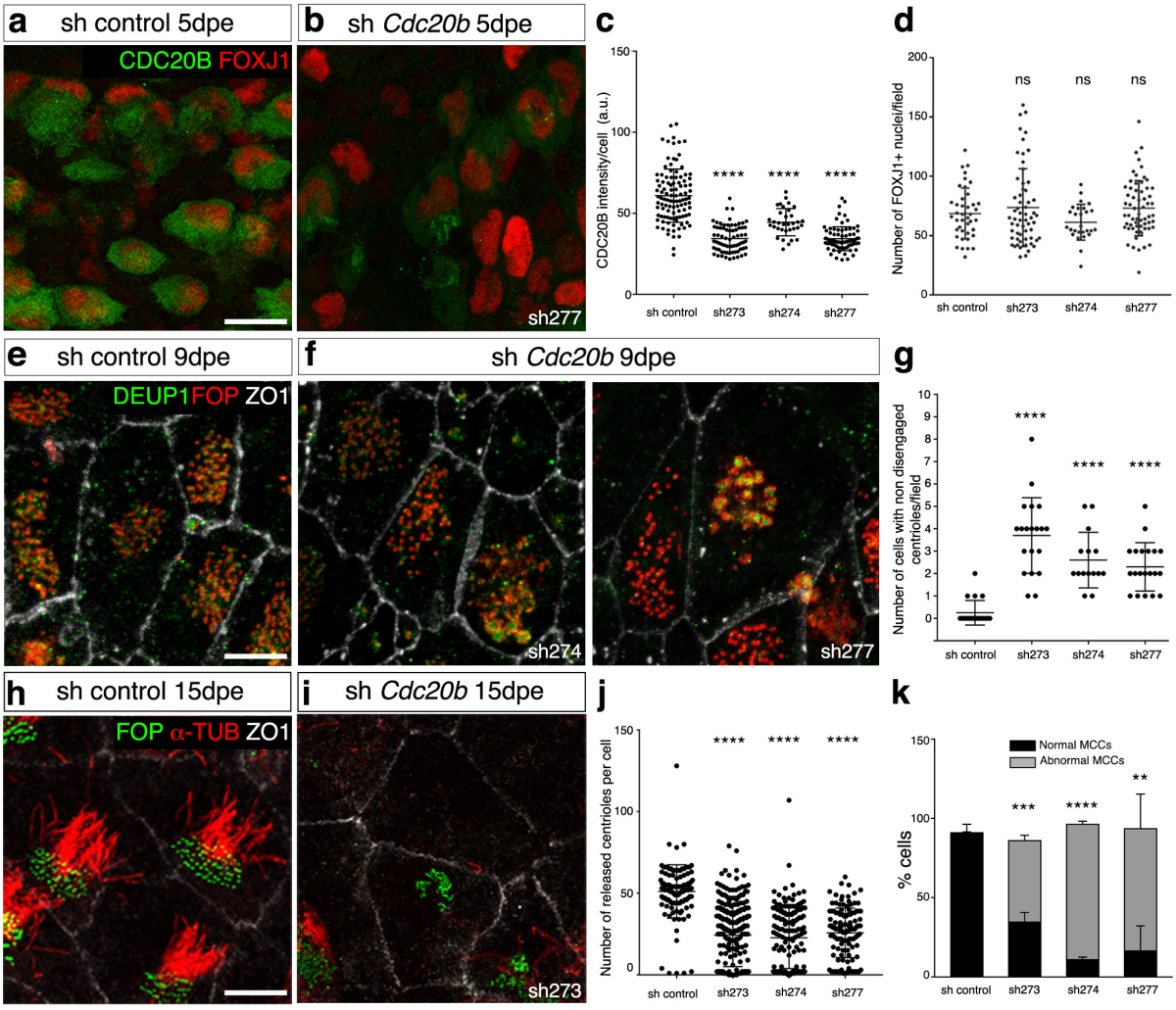

537

538 **Figure 4: CDC20B knockdown impairs centriole disengagement from deuterosomes and**

539 **ciliogenesis in mouse ependymal MCCs**.

540 (**a**,**b**) Ependyma were stained for CDC20B (green) and FOXJ1 (nuclear MCC fate marker, red)

541 5 days post electroporation (5dpe) of control shRNA (**a**) or *Cdc20b* shRNA (**b**). sh277 is

542 exemplified here, but all three *Cdc20b* shRNAs produced similar effects. (**c**) Graph showing

543 the quantification of CDC20B protein levels in cells at the deuterosomal stage at 5dpe.

544 Horizontal lines are mean values and vertical lines are standard deviations. (**d**) Histogram

545 showing the number of FOXJ1-positive nuclei observed for each field (dot), with mean values

546 (horizontal lines) and standard deviations (vertical lines). No significant variations were

547 observed between conditions, indicating that MCC fate acquisition was not affected by *Cdc20b*

548 knockdown. (**e**-**f**) Confocal pictures of 9dpe ependyma electroporated with control shRNA (**e**)

549 or *Cdc20b* shRNAs (**f**) and stained for DEUP1 (deuterosome, green), FOP (centrioles, red) and
550 ZO1 (cell junction, white). DEUP1 positive deuterosomes with non-disengaged FOP positive
551 centrioles were observed much more frequently in MCCs electroporated with *Cdc20b* shRNAs
552 compared to control shRNA. (**g**) Histogram showing the number of cells with non-disengaged
553 centrioles per field (dots), with mean values (horizontal bars) and standard deviations (vertical
554 lines). (**h-i**) Confocal pictures of 15dpe ependyma stained for FOP (centrioles, green), α-
555 Tubulin (α-TUB, cilia, red) and ZO1 (cell junction, white) showing the morphology of normal
556 MCCs in shRNA control condition (**h**), and examples of defects observed in MCCs treated with
557 sh *Cdc20b* (**i**). (**j**) Histogram showing the number of released centrioles per cell (dots), with
558 mean values (horizontal bars) and standard deviations (vertical lines). (**k**) Bar graph showing
559 the percentage of normal and abnormal MCCs. MCCs were scored abnormal when they did not
560 display organized centriole patches associated to cilia. Scale bars: 20μm (**a**), 5μm (**e**, **i**).
561

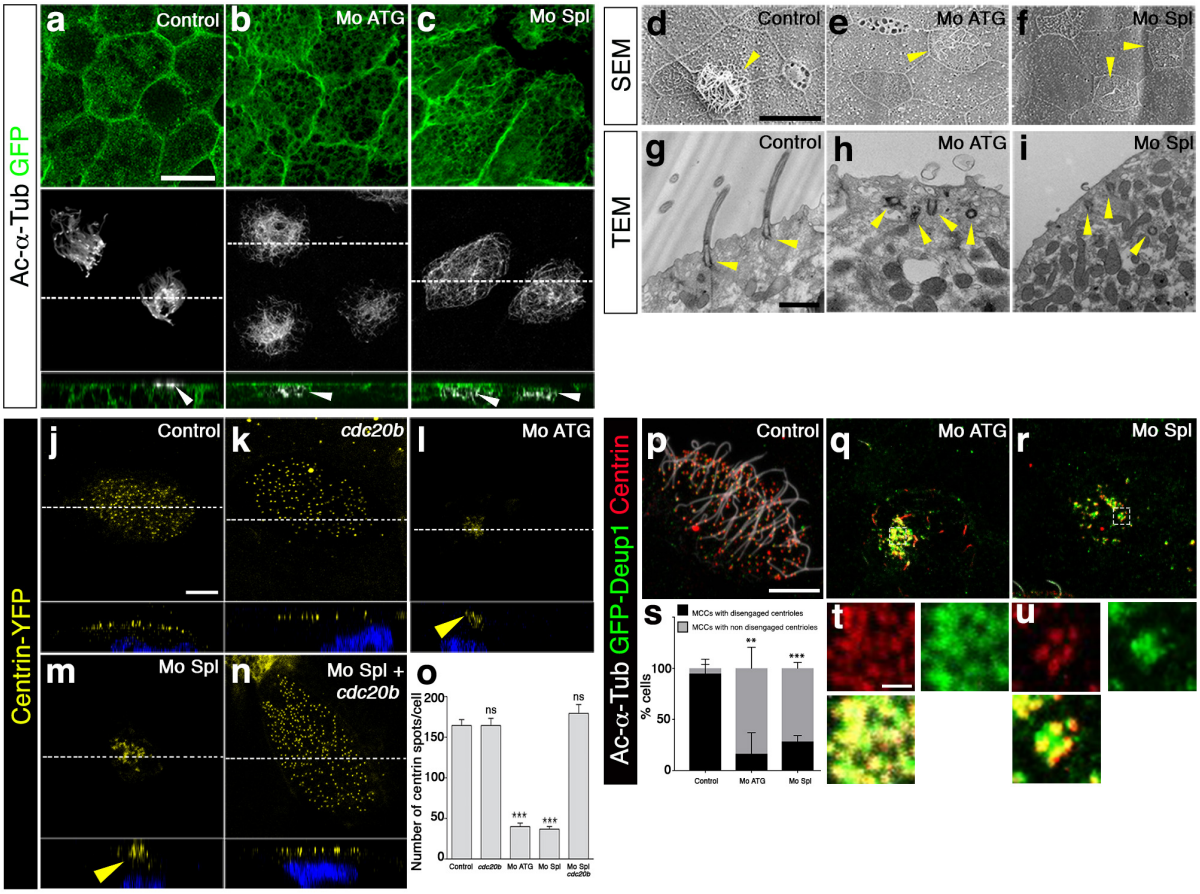

562

563 **Figure 5: *cdc20b* knockdown impairs centriole disengagement, docking and ciliogenesis**

564 **in *Xenopus* epidermal MCCs.**

565 (**a-c**) 8-cell embryos were injected in presumptive epidermis with *GFP-CAAX* mRNA and

566 *cdc20b* morpholinos, as indicated. Embryos at tailbud st25 were processed for fluorescent

567 staining against GFP (injection tracer, green) and Acetylated-α-Tubulin (Ac-α-Tub, cilia,

568 white). White dotted lines indicate the position of orthogonal projections shown in bottom

569 panels. Note that *cdc20b* morphant MCCs display cytoplasmic filaments but do not grow cilia

570 (white arrowheads). (**d-f**) Scanning Electron Microscopy (SEM) of control (**d**) and *cdc20b*

571 morphant (**e**,**f**) embryos at tadpole st31. Yellow arrowheads point at normal (**d**) and defective

572 MCCs (**e**,**f**). (**g-i**) Transmission Electron Microscopy (TEM) of control (**g**) and *cdc20b*

573 morphant (**h**,**i**) embryos at tailbud st25. Yellow arrowheads point at normally docked basal

574 bodies supporting cilia (**g**) and undocked centrioles unable to support cilia (**h**,**i**). (**j-n**) 8-cell

575 embryos were injected in presumptive epidermis with *centrin-YFP* mRNA, *cdc20b*
576 morpholinos, and *cdc20b* mRNA, as indicated. Centrin-YFP fluorescence was observed
577 directly to reveal centrioles (yellow). Nuclei were revealed by DAPI staining in blue. White
578 dotted lines indicate the position of orthogonal projections shown in bottom panels. Yellow
579 arrowheads point at undocked centrioles. (**o**) Bar graph showing the number of BBs per MCC,
580 as counted by Centrin-YFP dots. *cdc20b* knockdown significantly reduced the number of BBs
581 per cell, and this defect could be corrected by *cdc20b* co-injection with Mo Spl. (**p-u**) Embryos
582 were injected with *Multicilin-hGR* and *GFP-Deup1* mRNAs, treated with dexamethasone at
583 gastrula st11 to induce Multicilin activity, and immunostained at neurula st23 against
584 Acetylated-α-tubulin (cilia, white), GFP (deuterosomes, green) and Centrin (centrioles, red).
585 (**p**) Control cells showed individual centrioles, many of which had initiated ciliogenesis. Note
586 that Deup1-positive deuterosomes were no longer visible at this stage. (**q**,**r**,**t**,**u**) *cdc20b*
587 morphant MCCs showed procentrioles still engaged on deuterosomes and lacked cilia. (**s**) bar
588 graph showing the percentage of cells that completed or not centriole disengagement. Scale
589 bars: 20µm (**a**, **d**), 1µm (**g**, **t**), 5µm (**j**, **p**).
590

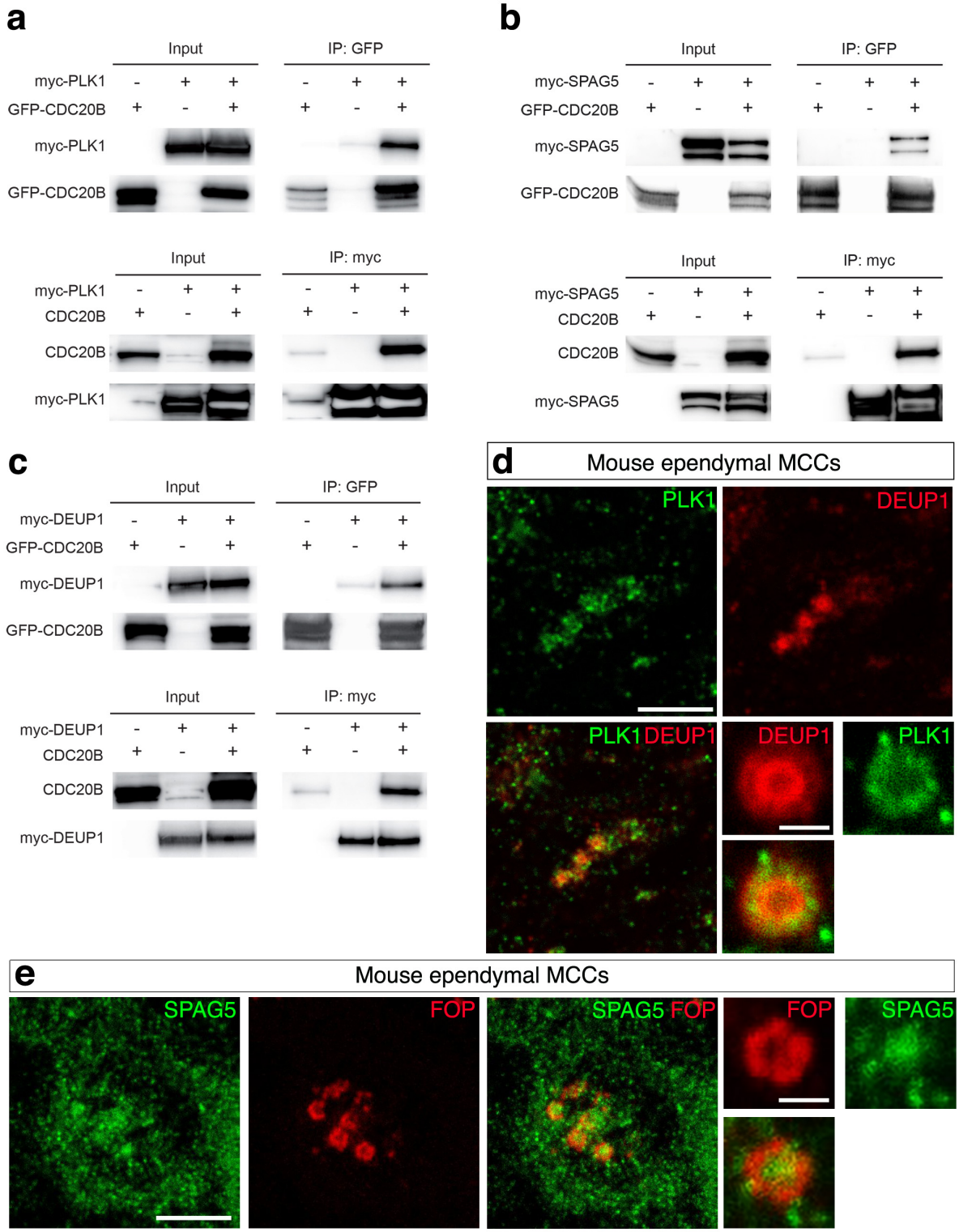

591

592 **Figure 6: CDC20B interacts with PLK1, SPAG5 and DEUP1**

593 (**a-c**) Co-immunoprecipitations of PLK1, SPAG5 and DEUP1 with CDC20B were tested after

594 transfections of different constructs in HEK cells, indicated at the top of each panel. Proteins

595 (left legend) were revealed by immunoblotting. (**d**) Maturing mouse ependyma were
596 immunostained for the indicated proteins, and pictures were taken with a confocal microscope.
597 PLK1 and SPAG5 are expressed in maturing MCCs. High magnifications show that PLK1 is
598 enriched in the perideuterosomal region, while SPAG5 is enriched in the deuterosome core.
599 Scale bars: 5µm (**d**, **e**, large view), 1µm (**d**, **e**, high magnification).
600

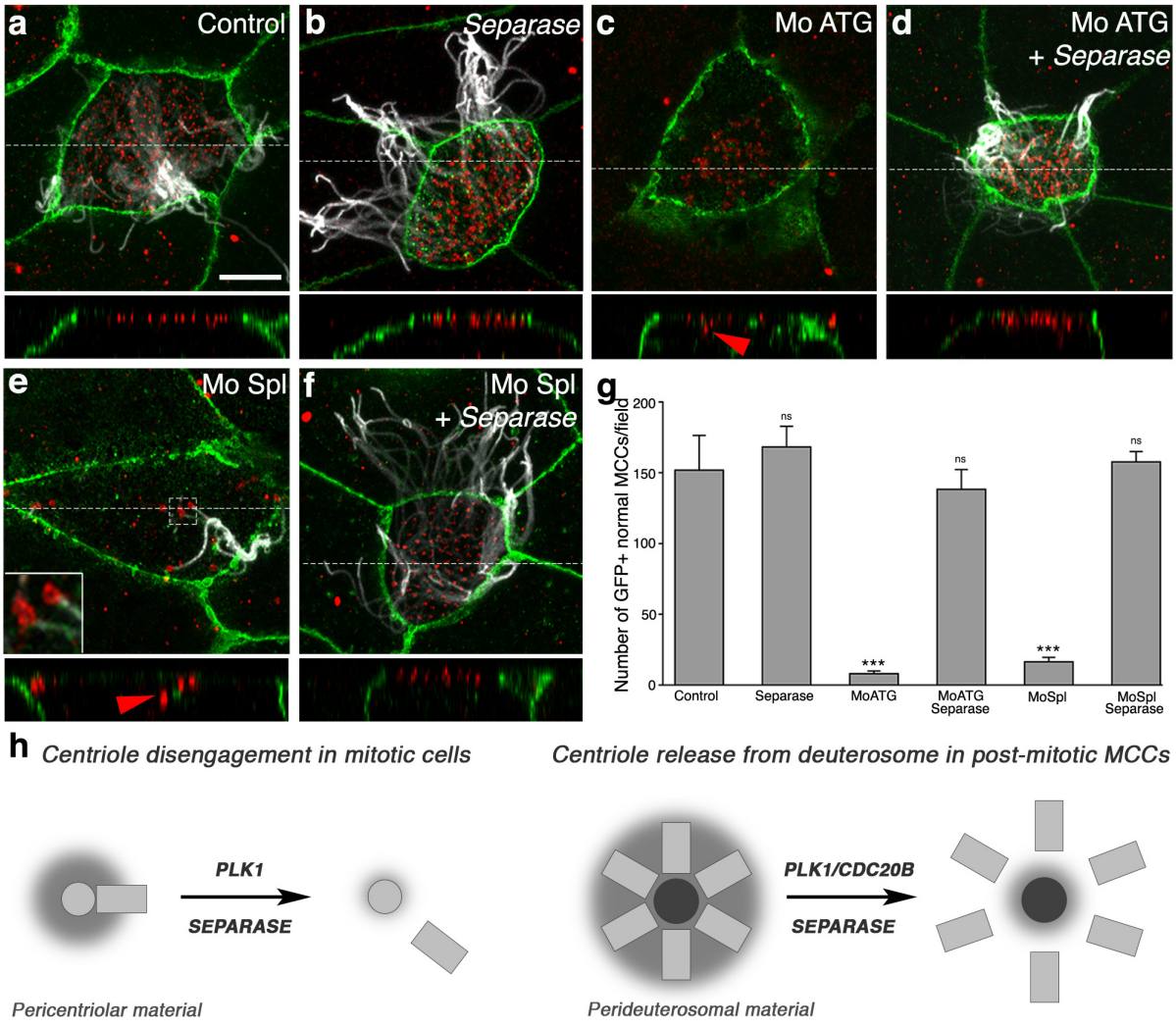

601

602 **Figure 7: Separase overexpression rescues multiciliogenesis in absence of Cdc20b.**

603 (**a-f**) 8-cell *Xenopus* embryos were injected in the presumptive epidermis with *GFP-gpi* mRNA,
604 *cdc20b* morpholinos, and human *Separase* mRNA, as indicated. Embryos were fixed at tailbud
605 st25 and immunostained against GFP (injection tracer, green), Acetylated-α-Tubulin (cilia,
606 white) and ɣ-Tubulin (BBs, red). White dotted lines indicate the position of orthogonal
607 projections shown in bottom panels. Red arrowheads point undocked BBs. Left inset in (**e**)
608 shows zoom on clustered centrioles. (**g**) Bar graph showing the number of properly ciliated
609 MCCs among injected cells, per field of observation. Counting was performed on pictures taken
610 at low magnification (20x), in order to score a large number of cells. Separase overexpression
611 fully rescued multiciliogenesis in *cdc20b* morphant MCCs. Scale bars: 5µm (**a**). (**h**) Model

612 illustrating the analogy between centriole disengagement in mitotic cells and centriole release
613 from deuterosomes in post-mitotic MCCs.
614
615 **Materials and Methods**
616 Subjects/human samples
617 Inferior turbinates were from patients who underwent surgical intervention for nasal obstruction
618 or septoplasty (provided by L. Castillo, Nice University Hospital, France). The use of human
619 tissues was authorized by the bioethical law 94-654 of the French Public Health Code and
620 written consent from the patients.
621
622 Single-cell RNA sequencing of HAECs
623 HAECs were cultured as previously described[23]. They were induced to differentiate at the air-
624 liquid interface for 14 days, which corresponds to the maximum centriole multiplication stage.
625 Cells were incubated on Transwell® (Corning®, NY 14831 USA) with 0.1% protease type
626 XIV from *Streptomyces griseus* (Sigma-Aldrich) in HBSS (Hanks' balanced salts) for 4 hours
627 at 4°C. Cells were gently detached from the Transwells by pipetting and then transferred to a
628 microtube. 50 units of DNase I (EN0523 Thermo Fisher Scientific) per 250µl, were directly
629 added and cells were further incubated at room temperature for 10 min. Cells were centrifuged
630 (150g for 5 min) and resuspended in 500 µL HBSS 10% Fetal Bovine Serum (Gibco),
631 centrifuged again (150g for 5 min) and resuspended in 500 µL HBSS before being mechanically
632 dissociated through a 26G syringe (4 times). Finally, cell suspensions were filtered through a
633 Scienceware® Flowmi™ Cell Strainer (40µm porosity), centrifuged (150g for 5 min) and
634 resuspended in 500 µL of cold HBSS. Cell concentration measurements were performed with
635 Scepter™ 2.0 Cell Counter (millipore) and Countess™ automated cell counter (ThermoFisher
636 Scientific). Cell viability was checked with Countess™ automated cell counter (ThermoFisher

637 Scientific). All steps except the DNAse I incubation were performed on ice. For the cell capture
638 by the 10X genomics device, the cell concentration was adjusted to 300 cells/µl in HBSS aiming
639 to capture 1500 cells. We then followed the manufacturer's protocol (Chromium™ Single Cell
640 3' Reagent Kit, v2 Chemistry) to obtain single cell 3' libraries for Illumina sequencing. Libraries
641 were sequenced with a NextSeq 500/550 High Output v2 kit (75 cycles) that allows up to
642 *91* cycles of paired-end sequencing: the forward read had a length of 26 basse that included the
643 cell barcode and the UMI; the reverse read had a length of 57 bases that contained the cDNA
644 insert. CellRanger Single-Cell Software Suite v1.3 was used to perform sample demultiplexing,
645 barcode processing and single-cell 3′ gene counting using standards default parameters and
646 human build hg19. Additional analyses were performed using R. Pseudotemporal ordering of
647 single cells was performed with the last release of the Monocle package[45]. Cell cycle scores
648 were calculated by summing the normalized intensities of genes belonging to phase-specific
649 gene sets then centered and scaled by phase. Gene sets for each phase were curated from
650 previously described sets of genes[46] (Supplementary Table 1). Data was submitted to the GEO
651 portal under series reference GSE103518. Data shown in Figure 1 is representative of 4
652 independent experiments performed on distinct primary cultures.
653
654 RNA sequencing of HAECs
655 For Figure S3A, three independent HAEC cultures (HAEC1, HAEC2, HAEC3) were triggered
656 to differentiate in air-liquid interface (ALI) cultures for 2 days (ALI day 2, undifferentiated),
657 ALI day 14 (first cilia) or ALI day 28 (well ciliated). RNA was extracted with the miRNeasy
658 mini kit (Qiagen) following manufacturer's instructions. mRNA-seq was performed from 2 µg
659 of RNA that was first subjected to mRNA selection with Dynabeads® mRNA Purification Kit
660 (Invitrogen). mRNA was fragmented 10 min at 95°C in RNAseIII buffer (Invitrogen) then
661 adapter-ligated, reverse transcribed and amplified (6 cycles) with the reagents from the

NEBNext Small RNA Library Prep Set for SOLiD. Small RNA-seq was performed from 500 ng RNA with the NEBNext Small RNA Library Prep Set for SOLiD (12 PCR cycles) according to manufacturer's instructions. Both types of amplified libraries were purified on Purelink PCR micro kit (Invitrogen), then subjected to additional PCR rounds (8 cycles for RNA-seq and 4 cycles for small RNA-seq) with primers from the 5500 W Conversion Primers Kit (Life Technologies). After Agencourt® AMPure® XP beads purification (Beckman Coulter), libraries were size-selected from 150 nt to 250 nt (for RNA-seq) and 105 nt to 130 nt (for small RNA-seq) with the LabChip XT DNA 300 Assay Kit (Caliper Lifesciences), and finally quantified with the Bioanalyzer High Sensitivity DNA Kit (Agilent). Libraries were sequenced on SOLiD 5500XL (Life Technologies) with single-end 50b reads. SOLiD data were analyzed with lifescope v2.5.1, using the small RNA pipeline for miRNA libraries and whole transcriptome pipeline for RNA-seq libraries with default parameters. Annotation files used for production of raw count tables correspond to Refseq Gene model v20130707 for mRNAs and miRBase v18 for small RNAs. Data generated from RNA sequencing were then analyzed with Bioconductor (http://www.bioconductor.org) package DESeq and size-factor normalization was applied to the count tables. Heatmaps were generated with GenePattern using the "Hierarchical Clustering" Module, applying median row centering and Euclidian distance.

Re-analysis of *Xenopus* E2F4 Chip-seq and RNA-seq

RNA-seq (samples GSM1434783 to GSM1434788) and ChIP-seq (samples GSM1434789 to GSM1434792) data were downloaded from GSE59309. Reads from RNA-seq were aligned to the *Xenopus laevis* genome release 7.1 using TopHat2[47] with default parameters. Quantification of genes was then performed using HTSeq-count[48] release 0.6.1 with "-m intersection-nonempty" option. Normalization and statistical analysis were performed using Bioconductor package DESeq2[49]. Differential expression analysis was done between Multicilin-hGR alone

687 versus Multicilin-hGR in the presence of E2f4ΔCT. Reads from ChIP-seq were mapped to the
688 *Xenopus laevis* genome release 7.1 using Bowtie2[50]. Peaks were called and annotated according
689 to their positions on known exons with HOMER[51]. Peak enrichments of E2F4 binding site in
690 the promoters of centriole genes and cell cycle genes[9] were estimated in presence or absence of
691 Multicilin and a ratio of E2F4 binding (Multicilin vs no Multicilin) was calculated.
692
693 Promoter reporter studies
694 The human *CDC20B* promoter was cloned into the pGL3 Firefly Luciferase reporter vector
695 (Promega) with SacI and NheI cloning sites. The promoter sequenced ranged from -1073 to
696 +104 relative to the transcription start site. 37.5 ng of pGL3 plasmid were applied per well.
697 pCMV6-Neg, pCMV6-E2F1 (NM_005225) and pCMV6-E2F4 (NM_001950) constructs were
698 from Origene. 37.5 ng of each plasmid was applied per well. 25 ng per well of pRL-CMV
699 (Promega) was applied in the transfection mix for transfection normalization (Renilla
700 luciferase). HEK 293T cells were seeded at 20 000 cells per well on 96-well plates. The
701 following day, cells were transfected with the indicated plasmids (100 ng of total DNA) with
702 lipofectamine 3000 (Invitrogen). After 24 hours, cells were processed with the DualGlo kit
703 (Promega) and luciferase activity was recorded on a plate reader.
704
705 Proximity ligation Assays
706 Fully differentiated HAECs were dissociated by incubation with 0.1% protease type XIV from
707 *Streptomyces griseus* (Sigma-Aldrich) in HBSS (Hanks' balanced salts) for 4 hours at 4°C. Cells
708 were gently detached from the Transwells by pipetting and then transferred to a microtube.
709 Cells were then cytocentrifuged at 300 rpm for 8 min onto SuperFrostPlus slides using a
710 Shandon Cytospin 3 cytocentrifuge. Slides were fixed for 10 min in methanol at -20°C for
711 Centrin2 and ZO1 assays, and for 10 min in 4% paraformaldehyde at room temperature and

712 then permeabilized with 0.5% Triton X-100 in PBS for 10 min for Acetylated-α-tubulin assays.
713 Cells were blocked with 3% BSA in PBS for 30 min. The incubation with primary antibodies
714 was carried out at room temperature for 2 h. Then, mouse and rabbit secondary antibodies from
715 the Duolink® Red kit (Sigma-Aldrich) were applied and slides were processed according to
716 manufacturer's instructions. Images were acquired using the Olympus Fv10i confocal imaging
717 systems with 60X oil immersion objective and Alexa 647 detection parameters.
718
719 Animals
720 All experiments were performed following the Directive 2010/63/EU of the European
721 parliament and of the council of 22 September 2010 on the protection of animals used for
722 scientific purposes. Experiments on *Xenopus laevis* and mouse were approved by the 'Direction
723 départementale de la Protection des Populations, Pôle Alimentation, Santé Animale,
724 Environnement, des Bouches du Rhône' (agreement number F 13 055 21). Mouse experiments
725 were approved by the French ethical committee n°14 (permission number: 62-12112012).
726 Timed pregnant CD1 mice were used (Charles Rivers, Lyon, France).
727
728 Immunostaining on mouse ependyma
729 Immunostaining on ependyma preparations were performed as previously described [52]. Briefly,
730 dissected brains were subjected to 12 min fixation in 4% paraformaldehyde, 0.1% Triton X-
731 100, blocked 1 hour in PBS, 3% BSA, incubated overnight with primary antibodies diluted in
732 PBS, 3% BSA, and incubated 1 h with secondary antibodies at room temperature. Ependyma
733 were dissected further and mounted with Mowiol before imaging using an SP8 confocal
734 microscope (Leica microsystems) equipped with a 63x oil objective. The same protocol was
735 used to prepare samples for super-resolution acquisition. Pictures were acquired with a TCS
736 SP8 STED 3X microscope equipped with an HC PL APO 93X/1.30 GLYC motCORR™

737 objective (Leica microsystems). Pericentrin was revealed using Alexa 514 (detection 535-
738 564nm, depletion 660nm), γ-tubulin was revealed using Alexa 568 (detection 582-667nm,
739 depletion 775), and FOP was revealed using Alexa 488 (detection 498-531nm, depletion
740 592nm). Pictures were deconvoluted using Huygens software. Maximum intensity projection
741 of 3 deconvoluted pictures is presented in Figure 4G. Primary antibodies: rabbit anti-CDC20B
742 (1:500; Proteintech), mouse IgG anti-PLK1 (1:500; Thermo Fisher), rabbit anti-Pericentrin
743 (1:500, Abcam), mouse IgG2a anti-Securin (1:100; Abcam), rabbit anti-Separase (1:200;
744 Abcam), mouse IgG1 anti-FoxJ1 (1:1000; eBioscience), rabbit anti-Deup1 (1:1000; kindly
745 provided by Dr Xueliang Zhu), rabbit anti-Deup1 (1:250; Proteintech), mIgG1 anti-γ-Tubulin
746 (clone GTU88) (1:250; Abcam), rabbit anti-ZO1 (1:600; Thermo Fisher Scientific), rabbit anti-
747 Spag5 (1:500; Proteintech), mouse IgG1 anti-ZO1 (1:600; Invitrogen), mouse IgG2b anti-
748 FGFR1OP (FOP) (1:2000; Abnova), mouse IgG1 anti-α-tubulin (1:500; Sigma-Aldrich).
749 Secondary antibodies: Alexa Fluor 488 goat anti-rabbit (1:800; Thermo Fisher Scientific),
750 Alexa Fluor 647 goat anti-rabbit (1:800; Thermo Fisher Scientific), Alexa Fluor 514 goat anti-
751 rabbit (1:800; Thermo Fisher Scientific), Alexa Fluor 488 goat anti-mouse IgG2b (1:800;
752 Thermo Fisher Scientific), Alexa Fluor 568 goat anti-mouse IgG2b (1:800; Thermo Fisher
753 Scientific), Alexa Fluor 488 goat anti-mouse IgG2a (1:800; Thermo Fisher Scientific), Alexa
754 Fluor 568 goat anti-mouse IgG1 (1:800; Thermo Fisher Scientific), Alexa Fluor 647 goat anti-
755 mouse IgG1 (1:800; Thermo Fisher Scientific).
756
757 Mouse constructs
758 Expression constructs containing shRNA targeting specific sequences in the CDC20B coding
759 sequence under the control of the U6 promoter were obtained from Sigma-Aldrich (ref.
760 TRCN0000088273 (sh273), TRCN0000088274 (sh274), TRCN0000088277 (sh277)). PCX-
761 mcs2-GFP vector (Control GFP) kindly provided by Xavier Morin (ENS, Paris, France), and

U6 vector containing a validated shRNA targeting a specific sequence in the NeuroD1 coding sequence[53](Control sh, ref. TRCN0000081777, Sigma-Aldrich) were used as controls for electroporation experiments.

Postnatal mouse brain electroporation

Postnatal mouse brain electroporation was performed as described previously[54]. Briefly, P1 pups were anesthetized by hypothermia. A glass micropipette was inserted into the lateral ventricle, and 2 µl of plasmid solution (concentration 3µg/µl) was injected by expiratory pressure using an aspirator tube assembly (Drummond). Successfully injected animals were subjected to five 95V electrical pulses (50 ms, separated by 950 ms intervals) using the CUY21 edit device (Nepagene, Chiba, Japan), and 10 mm tweezer electrodes (CUY650P10, Nepagene) coated with conductive gel (Signagel, Parker laboratories). Electroporated animals were reanimated in a 37°C incubator before returning to the mother.

Statistical analyses of mouse experiments

Analysis of CDC20B signal intensity in deuterosomes (graph in Fig. 3b). For each category, >25 cells from two different animals were analyzed. Deuterosome regions were delineated based on FOP staining and the intensity of CDC20B fluorescent immunostaining was recorded using ImageJ software, and expressed as arbitrary units. Unpaired t test vs immature: p=0,0005 (intermediate,***); p<0,0001 (Mature, ****).

Analysis of *Cdc20b* shRNAs efficiency (Fig. 4c): For each cell at the deuterosomal stage, the intensity of CDC20B fluorescent immunostaining was recorded using ImageJ software and expressed as arbitrary units. Data are mean ± sem. Two independent experiments were analyzed. A minimum of 35 cells per condition was analyzed. n= 3, 4, 5 and 5 animals for sh

786 control, sh273, sh274 and sh277, respectively. Unpaired t test vs sh control: p<0.0001 (sh273,
787 sh274 and sh277 ****).
788 Analysis of the number of FOXJ1 positive cells at 5dpe (Fig. 4d): Unpaired t test vs sh control:
789 0.3961 (sh273, ns), 0.1265 (sh274, ns), 0.3250 (sh277, ns).
790 Analysis of the number of cells with non-disengaged centrioles at 9dpe (Fig. 4g): 15-20 fields
791 were analyzed per condition. n= 4, 4, 3, and 4 animals for sh control, sh273, sh274 and sh277,
792 respectively, from 2 independent experiments. Unpaired t test vs sh control: p<0.0001 (sh273,
793 sh274, sh277 ****).
794 Analysis of the number of centrioles per cell at 15dpe (Fig. 4j): >100 cells were analyzed per
795 condition. n= 3, 3, 3, and 3 animals for sh control, sh273, sh274 and sh277, respectively, from
796 2 independent experiments. Unpaired t test vs sh control: p<0.0001 (sh273, sh274, sh277 ****).
797 Analysis of ependymal cell categories at 15dpe (Fig. 4k): Data are mean ± sem from three
798 independent experiments. More than 500 cells were analyzed for each condition. n= 4, 4, 3, and
799 3 animals for sh control, sh273, sh274 and sh277, respectively. Unpaired t test vs sh control:
800 p= 0.0004 (sh273, ***), 0.0001 (sh274, ****), 0.0038 (sh277, **).
801
802 Mouse tracheal epithelial cells (MTECs)
803 MTECs cell cultures were established from the tracheas of 12 weeks old mice, according to the
804 procedure previously published[55], with the following modification: in differentiation medium,
805 NuSerum™ was replaced with Ultroser-G™ (Pall Corporation) and 10 µM DAPT (N-[N-(3,5-
806 difluorophenacetyl)-L- alanyl]-S-phenylglycine t-butyl ester) (Sigma) was added one day after
807 setting-up the air-liquid interface.
808
809 Immunostaining on HAECs and MTECs

Three days after setting-up the air-liquid interface, MTECs on Transwell membranes were pre-extracted with 0.5% Triton X-100 in PBS for 3 min, and then fixed with 4% paraformaldehyde in PBS for 15 min at room temperature. HAECs were treated 21 days after setting-up the air-liquid interface. They were fixed directly on Transwells with 100% cold methanol for 10 min at -20°C (for CDC20B and Centrin2 co-staining, Supplementary Fig. 4a,b) or with 4% paraformaldehyde in PBS for 15 min at room temperature (for CDC20B single staining, Supplementary Fig. 4c). All cells were then permeabilized with 0.5% Triton X-100 in PBS for 5 min and blocked with 3% BSA in PBS for 30 min. The incubation with primary and secondary antibodies was carried out at room temperature for 2 h and 1 h, respectively. Nuclei were stained with 4,6-diamidino-2-phenylindole (DAPI). Transwell membranes were cut with a razor blade and mounted with ProLong Gold medium (Thermofisher). Primary antibodies: rabbit anti-CDC20B (1:500; Proteintech), rabbit anti-DEUP1 (1:500), anti-Centrin2 (Clone 20H5, 1:500; Millipore). Secondary antibodies: Alexa Fluor 488 goat anti-rabbit (1:1000; Thermo Fisher Scientific), Alexa Fluor 647 goat anti-mouse (1:1000; Thermo Fisher Scientific). For co-staining of CDC20B and DEUP1, CDC20B was directly coupled to CF^{TM} 633 with the Mix-n-Stain^{TM} kit (Sigma-Aldrich) according to the manufacturer's instruction. Coupled primary antibody was applied after secondary antibodies had been extensively washed and after a 30 min blocking stage in 3% normal rabbit serum in PBS.

Western blot and immunofluorescence analysis of transfected cells

Cos1 or Hela cells cells were grown in DMEM supplemented with 10% heat inactivated FCS and transfected with Fugene HD (Roche Applied Science) according to manufacturer's protocol. Transfected or control cells were washed in PBS and lysed in 50 mM Tris-HCl pH 7.5, 150 mM NaCl, 1mM EDTA, containing 1% NP-40 and 0.25% sodium deoxycholate (modified RIPA) plus a Complete Protease Inhibitor Cocktail (Roche Applied Science) on ice.

Cell extracts separated on polyacrylamide gels were transfered onto Optitran membrane (Whatman) followed by incubation with rabbit anti-mouse CDC20B (1:500, Proteintech) or homemade rabbit anti-*Xenopus* Cdc20b (1:300) antibody and horseradish peroxidase conjugated secondary antibody (Jackson Immunoresearch Laboratories). Signal obtained from enhanced chemiluminescence (Western Lightning ECL Pro, Perkin Elmer) was detected with MyECL Imager (Thermo Fisher Scientific).

For immunofluorescence staining, transfected cells were grown on glass coverslips and fixed for 6 min in methanol at -20°C. Cells were washed in PBS, blocked in PBS, 3% BSA and stained with rabbit anti-*Xenopus* Cdc20b (1:300) or rabbit anti-CFTR (1:200, Santa-Cruz Biotechnology) as a negative control, in blocking buffer. After washings in PBS 0.1% Tween-20, cells were incubated with Alexa fluor 488 donkey anti-rabbit antibody (Thermo Fisher Scientific), washed, and DNA was stained with 250 ng/ml DAPI. Coverslip were then rinsed and mounted in Prolong Gold antifade reagent (ThermoFisher Scientific) and confocal images were acquired by capturing Z-series with 0.3 µm step size on a Zeiss LSM 510 laser scanning confocal microscope.

Co-immunoprecipitation studies

Asynchronous HEK cells were rinsed on ice with chilled Ca++ and Mg++ free Dulbecco's PBS (DPBS, Invitrogen), harvested using acell scraper and lysed on ice for 5 min in lysis buffer (0.025M Tris, 0.15M NaCl, 0.001M EDTA, 1% NP-40, 5% glycerol; pH 7.4) supplemented with EDTA and Halt™ Protease and Phosphatase Inhibitor Cocktail (Pierce, Thermofisher). Lysates were clarified (12000g, 4°C, 10 min) and the protein concentrations were determined using the Bradford assay (Bio-Rad). Immunoprecipitations were performed with the Pierce co-immunoprecipitation kit (Pierce, Thermofisher) according to the manufacturer's instructions. For each immunoprecipitation, 1-1.5 mg of total lysate was precleared on a control column,

then incubated on columns coupled with 20 µg of anti-GFP or anti-c-myc-antibody (clone 9E10). Incubation was performed overnight at 4°C. Columns were washed and eluted with 50 µL elution buffer. Samples were denatured at 70°C for 10 min with Bolt™ LDS Sample Buffer and Bolt reducing agent, then separated on 4-12% gradient Bolt precast gels (Thermofisher), transferred onto nitrocellulose (Millipore), and subjected to immunoblot analysis using either anti-CDC20B (ProteinTech) or anti-c-myc antibody (clone 9E10). In Figure 6, note that the high level of expression of myc-PLK1 (**a**) and myc-SPAG5 (**b**) drained out locally the ECL reagent at the peak of the protein. The resulting double bands correspond in fact to unique ones. Human SPAG5, subcloned into pCMV6-MT, was from OriGene. Human DEUP1 and PLK1 were cloned into pCS2-MT vector (Addgene). Human CDC20B was cloned into pEGFP-C1, pEGFP-N1 (Clontech) for the GFP fusion protein and pIRES-EYFP (Addgene) for the untagged protein.

In-Gel digestion, NanoHPLC, and Q-exactive*plus* analysis

For mass spectrometry analysis, protein spots were manually excised from the gel and destained with 100 µL of H2O/ACN (1/1). After 10 min vortexing, liquid was discarded and the procedure was repeated 2 times. They were rinsed with acetonitrile and dried under vacuum. Extracts were reduced with 50 µL of 10 mM dithiothreitol for 30 min at 56 °C, then alkylated with 15 µL of 55 mM iodoacetamide for 15 min at room temperature in the dark. They were washed successively by: i) 100 µL of H2O/ACN (1/1) (2 times) and ii) 100 µL of acetonitrile. Gel pieces were rehydrated in 60 µL of 50 mM NH_4HCO_3 containing 10 ng/µL of trypsin (modified porcine trypsin, sequence grade, Promega) incubated for one hour at 4°C. After the removal of trypsin, samples were incubated overnight at 37°C. Tryptic peptides were extracted with: i) 60 µL of 1% FA (formic acid) in water (10 min at RT), ii) 60 µL acetonitrile (10 min

884 at RT). Extracts were pooled, concentrated under vacuum, resuspended in 15 µL of aqueous
885 0.1% formic acid for NanoHPLC separation.
886 Separation was carried out using a nanoHPLC (Ultimate *3000,* Thermo Fisher Scientific). After
887 concentration on a µ-Precolumn Cartridge Acclaim PepMap 100 C_{18} (i.d. 5 mm, 5 µm, 100 Å,
888 Thermo Fisher Scientific) at a flow rate of 10 µL/min, using a solution of H_2O/ACN/FA
889 98%/2%/0.1%, a second peptide separation was performed on a 75 µm i.d. x 250 mm (3 µm,
890 100 Å) Acclaim PepMap 100 C_{18} column (Thermo Fisher Scientific) at a flow rate of 300
891 nL/min. Solvent systems were: (A) 100% water, 0.1% FA, (B) 100% acetonitrile, 0.08% FA.
892 The following gradient was used t = 0min 6% B; t = 3 min 6%B; t = 119min, 45% B; t = 120
893 min, 90% B; t = 130 min 90% B (temperature at 35°C).
894 NanoHPLC was coupled via a nanoelectrospray ionization source to the Hybrid Quadrupole-
895 Orbitrap High Resolution Mass Spectrometer (Thermo Fisher Scientific). MS spectra were
896 acquired at a resolution of 70 000 (200 m/z) in a mass range of 300−2000 m/z with an AGC
897 target 3e6 value of and a maximum injection time of 100ms. The 10 most intense precursor
898 ions were selected and isolated with a window of 2m/z and fragmented by HCD (Higher energy
899 C-Trap Dissociation) with normalized collision energy (NCE) of 27. MS/MS spectra were
900 acquired in the ion trap with an AGC target 2e5 value, the resolution was set at 17 500 at 200
901 m/z combined with an injection time of 100 ms.
902 Data were reprocessed using Proteome Discoverer 2.1 equipped with Sequest HT. Files were
903 searched against the Swissprot Homo sapiens FASTA database (update of February 2016). A
904 mass accuracy of ± 10 ppm was used to precursor ions and 0.02 Da for product ions. Enzyme
905 specificity was fixed to trypsin, allowing at most two miscleavages. Because of the previous
906 chemical modifications, carbamidomethylation of cysteines was set as a fixed modification and
907 only oxydation of methionine was considered as a dynamic modification. Reverse decoy

908 databases were included for all searches to estimate false discovery rates, and filtered using the
909 Percolator algorithm at a 1% FDR.
910
911 *Xenopus* embryo injections, plasmids, RNAs, and mopholinos
912 Eggs obtained from NASCO females were fertilized *in vitro*, dejellied and cultured as described
913 previously[56]. All injections were done at the 8-cell stage in one animal-ventral blastomere
914 (presumptive epidermis), except for electron microscopy analysis for which both sides of the
915 embryo was injected, and for RT-PCR analysis for which 2-cell embryos were injected.
916 *cdc20b* riboprobe was generated from *Xenopus laevis* cDNA. Full-length sequence was
917 subcloned in pGEM™-T Easy Vector Systems (Promega). For sense probe it was linearized by
918 SpeI and transcribed by T7. For antisense probe it was linearized by ApaI and transcribed by
919 Sp6 RNA polymerase. Synthetic capped mRNAs were produced with the Ambion
920 mMESSAGE mMACHINE Kit. pCS105/GFP-CAAX was linearized with AseI and mRNA
921 was synthesized with Sp6 polymerase. pCS2-mRFP and pCS2-GFP-gpi were linearized with
922 NotI and mRNA was synthesized with Sp6 polymerase. pCS-Centrin4-YFP (a gift from
923 Reinhard Köster, Technische Universität Braunschweig, Germany) was linearized with NotI
924 and mRNA was synthesized with Sp6 polymerase. pCS2-GFP-Deup1 and pCS2-
925 Multicilin(MCI)-hGR were kindly provided by Chris Kintner and the mRNAs were obtained
926 as described previously[8]. Embryos injected with *MCI-hGR* mRNA were cultured in
927 Dexamethasone 20µM in MBS 0,1X from st11 until fixation. pCS2-Separase wild-type and
928 phosphomutant 2/4 (protease dead, PD) were provided by Marc Kirchner and Olaf Stemann,
929 respectively; plasmids were linearized with NotI and mRNAs were synthesized with Sp6
930 polymerase. *Venus-cdc20b*, *cdc20b-Venus* and *cdc20b* were generated by GATEWAY™
931 Cloning Technology (GIBCO BRL) from *Xenopus laevis cdc20b* cDNA. *cdc20b* was also
932 subcloned in pCS2-RFP to make *RFP-cdc20b* and *cdc20b-RFP* fusions. All *cdc20b* constructs

were linearized with NotI and mRNAs were synthesized with Sp6 polymerase. Quantities of mRNA injected: 500pg for *GFP-CAAX*, *RFP*, *GFP-gpi, Separase* and *Separase(PD);* 25 to 500pg for *GFP-Deup1*; 40 to 500pg for *MCI-hGR*; 1ng for *Venus-cdc20b*, *cdc20b-Venus*, *cdc20b*, and *cdc20b-RFP*; 500pg to 1ng for *RFP-cdc20b.*

Two independent morpholino antisense oligonucleotides were designed against *cdc20b* (GeneTools, LLC). *cdc20b* ATG Mo: 5'-aaatcttctctaacttccagtccat-3', *cdc20b* Spl Mo 5'-acacatggcacaacgtacccacatc-3'. 20ng of MOs was injected per blastomere or 10ng of each Mo for co-injection.

PCR and Quantitative RT-qPCR

Xenopus embryos were snap frozen at different stages and stored at -80°C. Total RNAs were purified with a Qiagen RNeasy kit (Qiagen). Primers were designed using Primer-BLAST Software. PCR reactions were carried out using GoTaq® G2 Flexi DNA Polymerase (Promega). RT reactions were carried out using iScript™ Reverse Transcription Supermix for RT-qPCR (BIO-RAD). qPCR reactions were carried out using SYBRGreen on a CFX Biorad qPCR cycler. To check *cdc20b* temporal expression by qPCR we directed primers to exons 9/10 junction (Forward: 5'-ggctatgaattggtgcccg-3') and exons 10/11 junction (Reverse: 5'-gcagggagcagatctggg-3') to avoid amplification from genomic DNA. The relative expression of *cdc20b* was normalized to the expression of the housekeeping gene *ornithine decarboxylase* (*ODC*) for which primers were as follows: forward: 5'-gccattgtgaagactctctccattc-3': reverse: 5'-ttcgggtgattccttgccac-3'.

To check the efficiency of Mo SPL, expected to cause retention of intron1 in the mature mRNA of *cdc20b* we directed forward (5'-cctcccgagagttagagga-3') and reverse (5'-gcatgttgtactttctgctcca-3') primers in exon1 and exon2, respectively.

To check the expression of *p53* in morphants by qPCR, primers were as follows: forward: 5'-cgcagccgctatgagatgatt-3'; reverse: 5'-cacttgcggcacttaatggt-3'. The relative expression of p53 was normalized to Histone4 expression (H4) for which primers were as follows: forward: 5'-ggtgatgccctggatgttgt-3'; reverse: 5'-ggcaaaggaggaaaaggactg-3'.

Immunostainining on *Xenopus* embryos

Embryos were fixed in 4% paraformaldehyde (PFA) overnight at 4°C and stored in 100% methanol at -20°C. Embryos were rehydrated in PBT and washed in MABX (Maleic Acid Buffer + Triton X100 0,1% v/v). Next, embryos were incubated in Blocking Reagent (Roche) 2% BR + 15% Serum + MABX with respective primary and secondary antibodies. The anti-*Xenopus laevis* CDC20B antibody was obtained by rabbit immunization with the peptide SPDQRRIFSAAANGT (amino acids 495–509) conjugated to keyhole limpet hemocyanin, followed by affinity purification (Eurogentec). For immunofluorescence, embryos were fixed at RT in PFA 4% in PBS, and incubated in the CDC20B antibody diluted 1/150 in BSA 3% in PBS. For all experiments secondary antibodies conjugated with Alexa were used. GFP-CAAX in Fig. 5g was revealed using a rabbit anti-GFP antibody together with a secondary antibody coupled to HRP, which was revealed as described previously[23]. To mark cortical actin in MCCs, embryos were fixed in 4% paraformaldehyde (PFA) in PBT (PBS + 0,1% Tween v/v) for 1h at room temperature (RT), washed 3x10 min in PBT at RT, then stained with phalloidin-Alexa Fluor 555 (Invitrogen, 1:40 in PBT) for 4 h at RT, and washed 3x10 min in PBT at RT. Primary antibodies: mouse anti-Acetylated–α-Tubulin (Clone 6-11B-1, Sigma-Aldrich, 1:1000), rabbit anti-γ-Tubulin (Abcam, 1:500), mouse anti-γ-Tubulin (Clone GTU88, Abcam, 1:500), Chicken anti-GFP (2B scientific, 1:1000), rabbit anti-GFP (Torrey Pines Biolabs, 1:500), mouse anti-Centrin (Clone 20H5, EMD Millipore; 1:500). Secondary antibodies: Alexa Fluor 647 goat

anti-mouse IgG2a (1:500; Thermo Fisher Scientific), Alexa Fluor 488 goat anti-chicken (1:500; Thermo Fisher Scientific), Alexa Fluor 568 goat anti-rabbit (1:500; Thermo Fisher Scientific).

In situ hybridization on *Xenopus* embryos

Whole-mount chromogenic *in situ* hybridization was performed as described previously[56]. Whole-mount fluorescent *in situ* hybridization (FISH) was performed as described previously[57]. For single staining, all RNA probes were labeled with digoxigenin. For FISH on section, embryos were fixed in 4% paraformaldehyde (PFA), stored in methanol for at least 4 h at −20°C, then rehydrated in PBT (PBS + Tween 0.1% v/v), treated with triethanolamine and acetic anhydride, incubated in increasing sucrose concentrations and finally embedded with OCT (VWR Chemicals). 12µm-thick cryosections were made. Double FISH on sections was an adaptation of the whole-mount FISH method. 80ng of *cdc20b* digoxigenin-labeled sense and antisense riboprobes and 40ng of antisense *α-tubulin* fluorescein-labeled riboprobe[58] were used for hybridization. All probes were generated from linearized plasmids using RNA-labeling mix (Roche). FISH was carried out using Tyramide Signal Amplification – TSA TM Plus Cyanine 3/Fluorescein System (PerkinElmer). Antibodies: Anti-rabbit-HRP (Interchim, 1:5000), Anti-DigAP (Roche, 1:5000), Anti-DigPOD (Roche, 1:500), Anti-FluoPOD (Roche, 1:500).

Microscopy

Confocal: Flat-mounted epidermal explants were examined with a Zeiss LSM 780 confocal microscope. Four-colors confocal z-series images were acquired using sequential laser excitation, converted into single plane projection and analyzed using ImageJ software. Scanning Electron Microscopy (SEM): skin epidermis of *Xenopus* embryos from stage 37 was observed and analyzed into a digital imaging microscope (FEI TENEO). Embryos were processed as described previously[57]. Transmission Electron Microscopy (TEM): St25 embryos

were fixed overnight at 4°C in 2.5% glutaraldehyde, 2% paraformaldehyde, 0.1% tannic acid in a sodium cacodylate buffer 0.05 M pH7.3. Next, embryos were washed 3x15 min in cacodylate 0.05 M at 4°C. Post-fixation was done in 1% osmium buffer for 2 h. Next, embryos were washed in buffer for 15 min. Then, embryos were washed in water and dehydrated conventionally with alcohol, followed by a step in 70% alcohol containing 2% uranyl during 1 to 2 h at RT, or overnight at 4°C. After 3 times in 100% alcohol, completed with 3 washes of acetone. Next, embryos were included in classical epon resin, which was polymerized in oven at 60°C for 48 h. Sections of 80 nm were made and analyzed into an FMI TECNAI microscope with acceleration of 200kV.

Statistical analysis of *Xenopus* experiments

To quantify the effect of our different experiments, we applied One-way ANOVA analysis and Bonferroni's multiple comparisons test (t test). ***P<0.05; ns = not significant. Statistical analyses were done using GraphPad Prism 6.

Fig. 5o and Fig. S6k: 10 cells per condition were analyzed and the total number of Centrin-YFP or γ-tubulin positive spots per injected cell was counted.

Fig. 7g: 5 fields (20x zoom) per condition were analyzed, and the total number of properly ciliated MCCs based on acetylated α-tubulin staining among GFP positive cells per field was counted. Each field corresponded to a different embryo.

Fig. 5s : 160-200 cells per condition were analyzed. n= 6, 8, and 10 embryos from 3 independent experiments for control, Mo ATG and Mo Spl, respectively. Unpaired t test vs control: p=0,0037 (Mo ATG **) and 0,0004 (Mo Spl ***).

Supplementary figures and legends

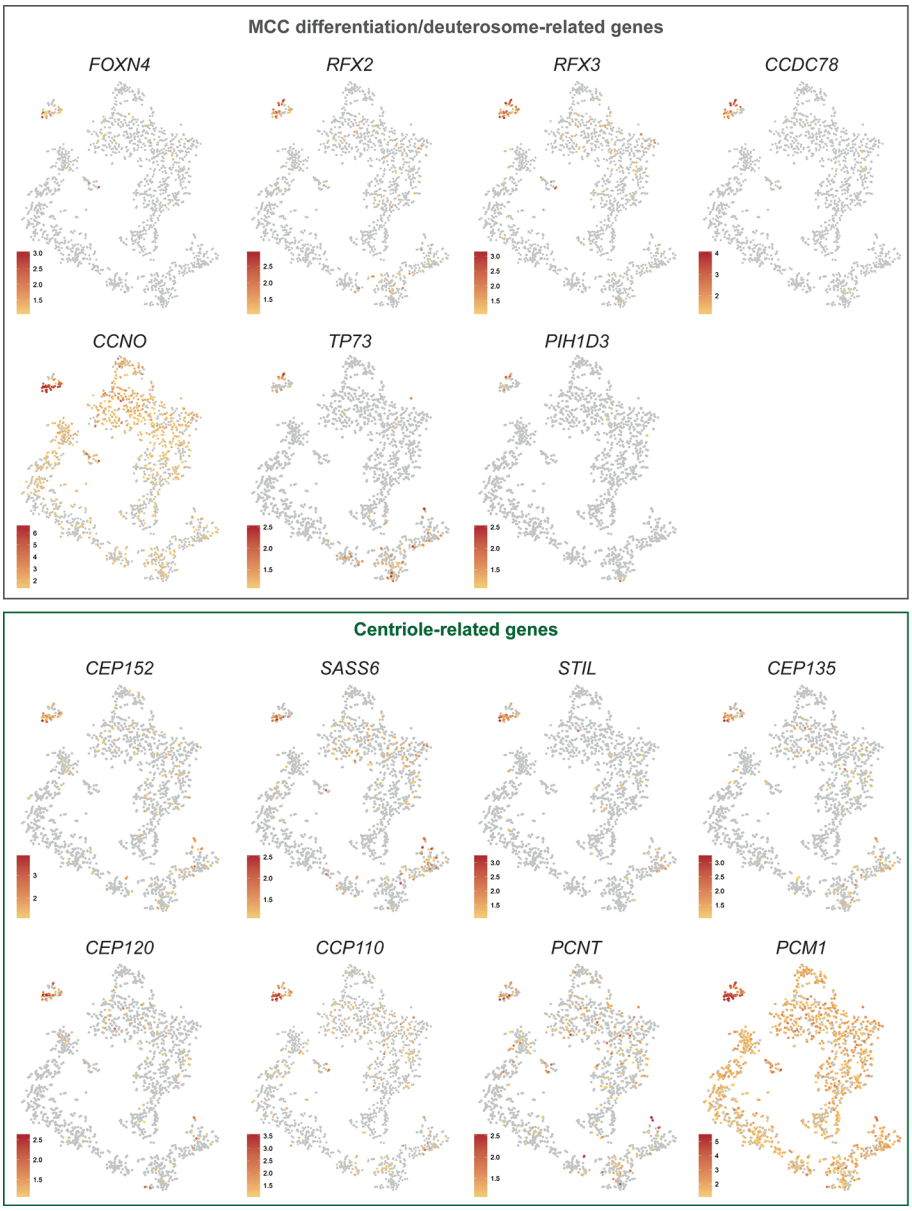

1031

1032

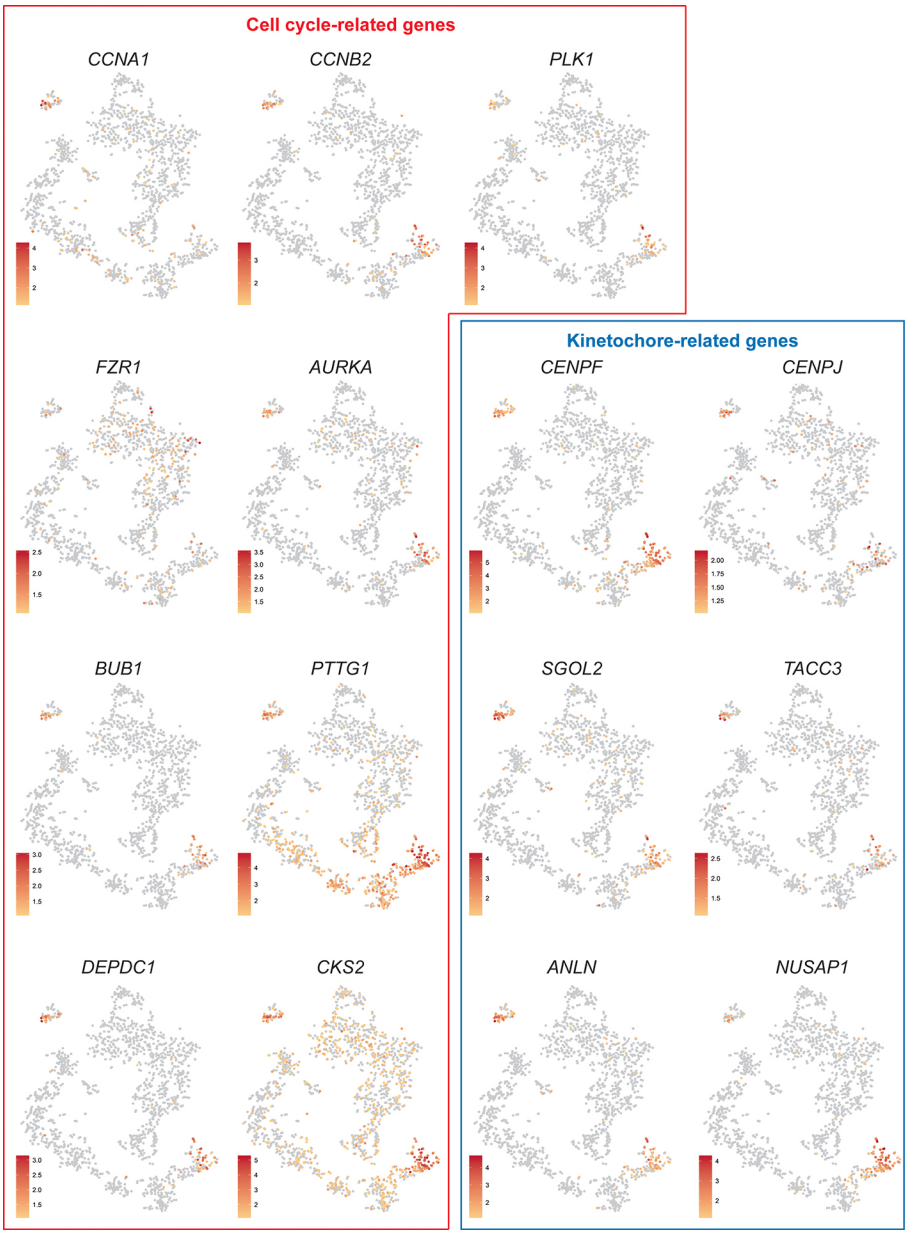

1033

1034 **Supplementary Figure 1: Single cell RNA-seq analysis of HAECs.**

1035 tSNE plots for a selection of genes expressed at the single-cell level, in deuterosomal-stage

1036 differentiating HAECs. Genes were grouped into functional categories.

1037

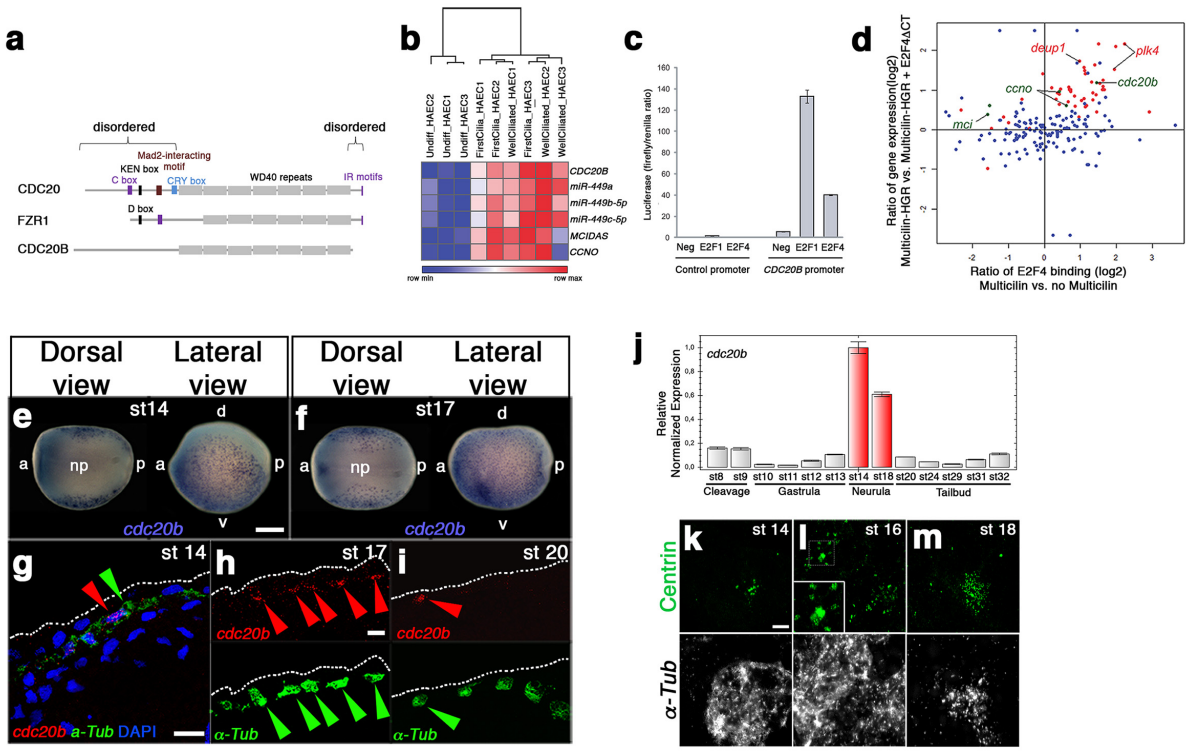

Supplementary Figure 2: Structure, regulation and sub-cellular localization of CDC20B. **Domain composition of CDC20 family members. (a)** The C box and IR motifs in CDC20 and FZR1 serve as APC/C binding domains. The KEN box and the Cry box in CDC20, and the D box in FZR1 are involved in their regulation by degradation. The Mad2-interacting motif in CDC20 is important for its regulation by the spindle assembly checkpoint. WD40 repeats are involved in substrate recognition. Note that CDC20B lacks degradation motifs and the APC/C binding domains present in CDC20 and FZR1. ***CDC20B* is induced during multiciliogenesis under the control of E2Fs/MCIDAS. (b)** Heatmap of gene expression measured by RNA-seq or small RNA-seq on 3 independent HAEC differentiation time courses (HAEC1 to HAEC3). Normalized read counts were Log2-transformed and median-centered by gene. Hierarchical clustering (Euclidian distance) was performed on samples. The scale color bar indicates the minimum and maximum values per row. (**c**) Promoter luciferase reporter assay. Promoter-associated firefly luciferase was normalized by constitutive renilla luciferase. Control and *CDC20B* promoter were co-expressed with a plasmid expressing E2F1 or E2F4, or a negative

control. Bars represent the average of 3 independent experiments. Error bars represent the standard deviation. (**d**) Ratio of gene expression (Multicilin-HGR vs. Multicilin-HGR +E2F4ΔCT) vs. ratio of E2F4 binding (Multicilin vs. no Multicilin). E2F4ΔCT prevents the formation of transcriptionally active Multicilin/E2F complexes. Centriole-related genes are highlighted in red. Genes from the multiciliary locus are highlighted in green. The graph was built by mapping and quantifying previously published raw data[9]. **CDC20B expression in *Xenopus* epidermis MCCs.** (**e**,**f**) *cdc20b* whole-mount *in situ* hybridization in early neurula st14 and st17, respectively. *cdc20b* mRNA is expressed in epidermal cells but not in the neural plate (np), as revealed on dorsal views. a: anterior, p: posterior, d: dorsal, v: ventral. (**g-i**) *cdc20b* (red) and *α-Tubulin* (α-*Tub,* green) double fluorescent *in situ* hybridization (FISH) on sectioned embryos at st14 (**g**), st17 (**h**) and st20 (**i**). Red and green arrows point immature MCCs co-expressing *cdc20b* and *α-Tub*. Nuclei are revealed by DAPI staining in blue. White dotted lines indicate the surface of the epidermis. Note that the majority of MCCs become negative for *cdc20b* expression at st20. (**j**) RT-qPCR showing the relative expression of *cdc20b* from st8 (mid-blastula transition) until tadpole st32 normalized with *ODC* expression. Red bars indicate the peak of *cdc20b* transcript accumulation between st14 and st18, when centriole amplification occurs. (**k-m**) To reveal the dynamics of centriole multiplication, MCCs were stained by α-*Tub* FISH and by immunostaining against Centrin. Multiple Centrin-positive foci were detected at st14, marking the onset of centriologenesis. Procentriole aggregates, presumably organized around deuterosomes were clearly visualized at st16 (inset). Dispersed multiple centrioles were detected at st18. Scale bars: 250µm (**e**), 20µm (**g**,**h**), 5µm (**k**).

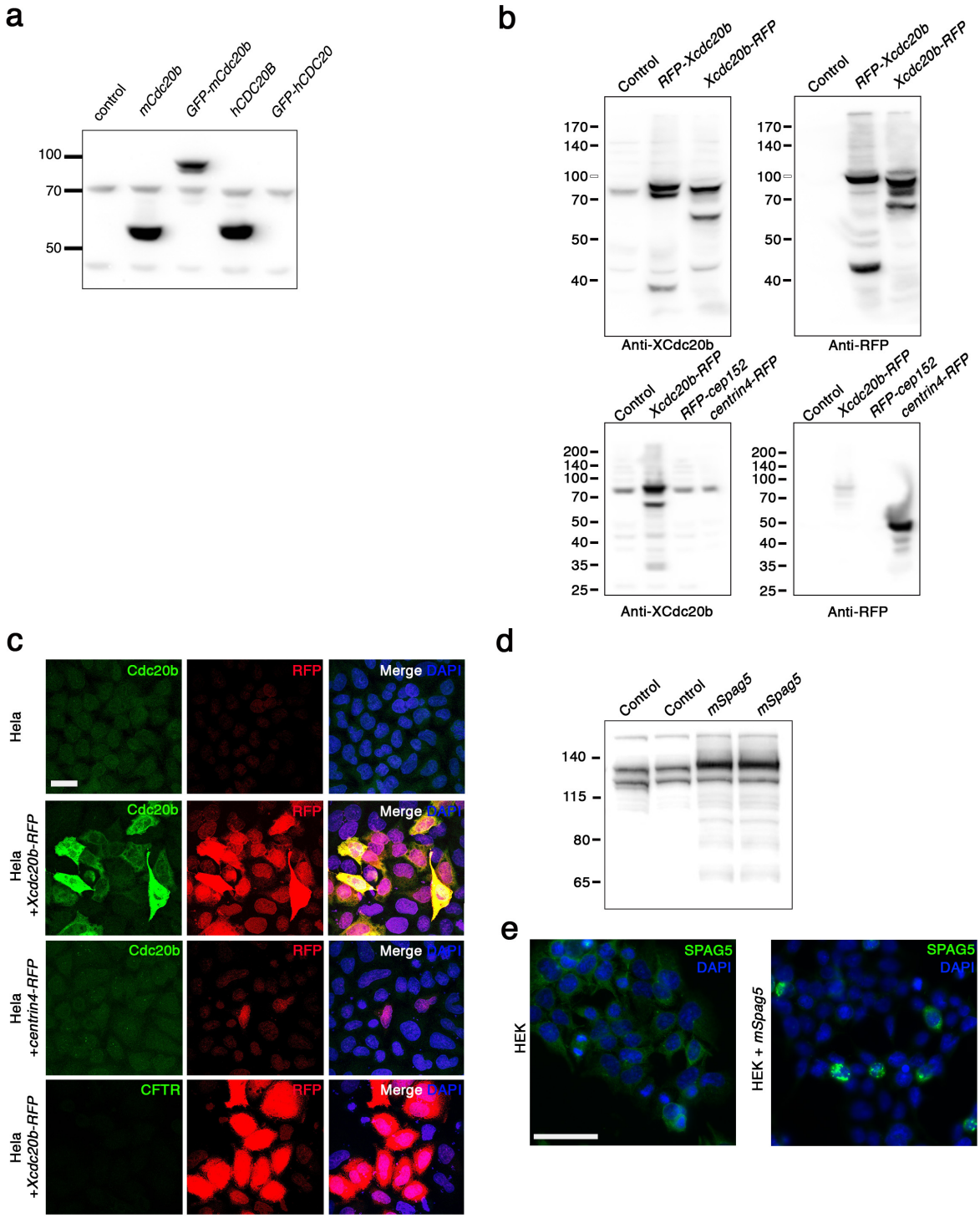

1075

1076 **Supplementary Figure 3: Antibody validations**

1077 **(a)** COS1 cells were transfected with vectors coding for the indicated proteins and immunoblot

1078 was performed using Proteintech rabbit antibody raised against human CDC20B. This antibody

1079 recognized human and mouse CDC20B but did not cross-react with human CDC20. (**b**) Hela

1080 cells were transfected with vectors coding for the indicated proteins and immunoblot was

performed using a custom-made rabbit antibody raised against *Xenopus* CDC20B. (**c**) Hela cells were transfected with vectors coding for the indicated proteins and immunostainings were performed using the antibodies indicated on the photographs. Note that the antibody directed against *Xenopus* CDC20B did not cross-react with the centriole marker Centrin4. (**d**) HEK cells were transfected in duplicate with pCMV6-mSpag5, lysed 24 hours later and western blot was performed using proteintech rabbit polyclonal antibody raised against human SPAG5. (**e**) HEK cells were transfected with pCMV6-mSpag5, fixed with methanol 24 hours later and immunostained using proteintech rabbit polyclonal antibody raised against human SPAG5. This antibody cross-reacted with mouse SPAG5. Scale bars: 20µm (**c**), 50µm (**e**).

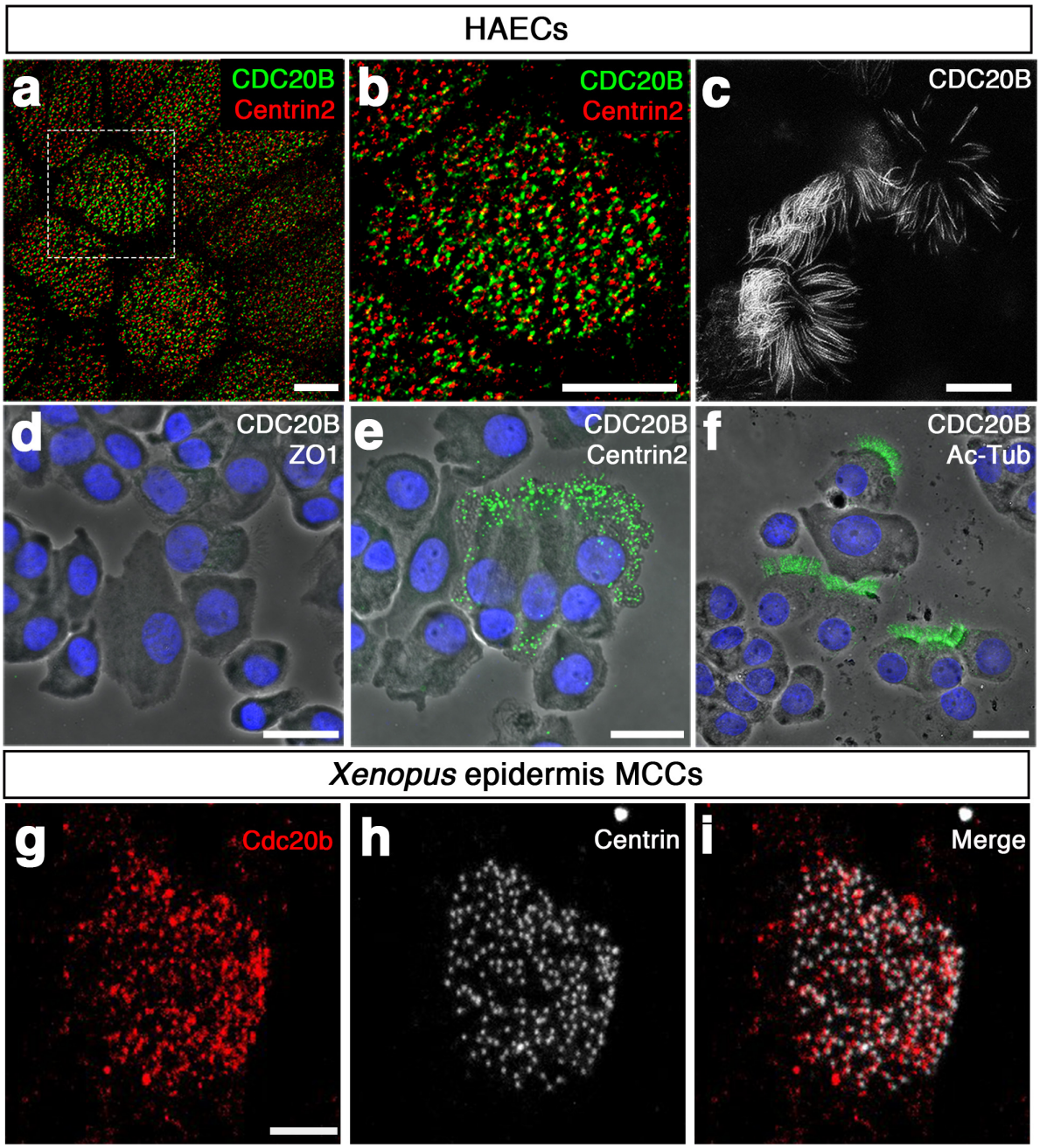

Supplementary Figure 4: CDC20B localization in mature MCCs.

(a-f) CDC20B sub-cellular localization in human mature MCCs. (a,**b**) ALI day 21 HAECs were fixed in methanol, and immunostained against CDC20B and Centrin2. STED super-resolution microscopy revealed the association of CDC20B to BBs. (**c**) ALI day 21 HAECs were fixed in paraformaldehyde, and immunostained against CDC20B. STED super-resolution microscopy revealed the association of CDC20B with cilia. (**d-f**) DuoLink Assays on fully

differentiated HAECs after cytospin. (**d**) Assay with CDC20B and ZO-1 antibodies was used as negative control. (**e**) Assay with CDC20B and Centrin2 (BBs) antibodies. (**f**) Assay with CDC20B and Acetylated-α-Tubulin (cilia) antibodies. Interaction between antibodies separated by less than 40nm generated green fluorescent signal. Nuclei are stained in blue. (**g-i**) **Cdc20b sub-cellular localization in *Xenopus* mature MCCs.** 4-cell *Xenopus* embryos were injected with *Multicilin-hGR* mRNA, induced with dexamethasone at stage 10.5 to activate Multicilin and immunostained for CDC20B (**g**) and Centrin (**h**) at stage 23. Scale bars: 5µm (**a-c**), 20µm (**d-f**), 5µm (**g**).

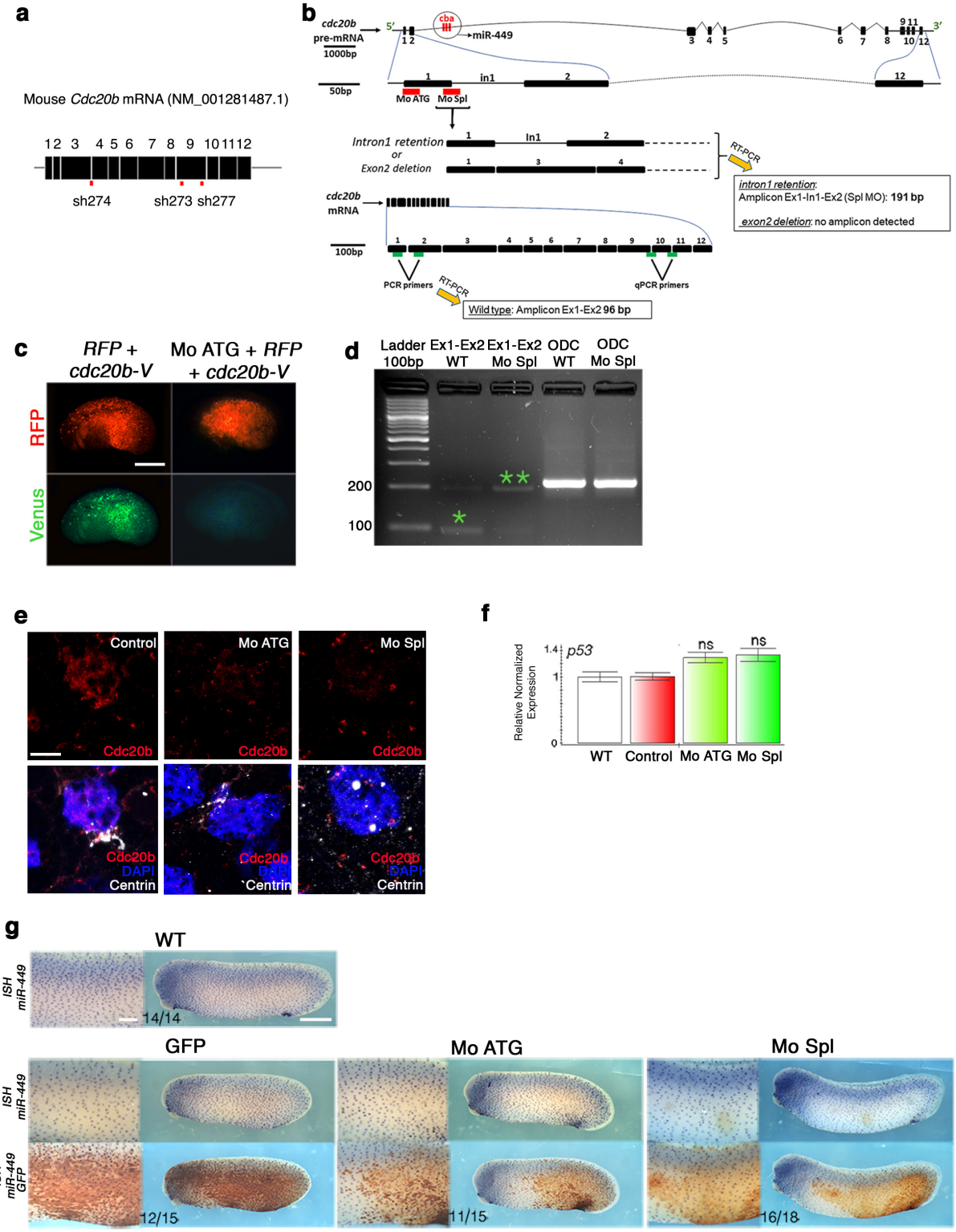

Supplementary Figure 5: *cdc20b* knockdown in mouse and *Xenopus*.

(**a**) Schematic representation of mouse *Cdc20b* mRNA and position of shRNAs used in this study. Note that sh274 targeted the junction between exons 3 and 4, ruling out possible

interference with the production of miR-449 molecules from the *Cdc20b* pre-mRNA. (**b**) Schematic representation of *Xenopus cdc20b* pre-mRNA with introns, exons and miR-449abc relative position and size. Red horizontal bars below exon1 show the position of *cdc20b* Mo ATG and Mo Spl. On the bottom, green horizontal bars indicate RT-PCR and qPCR primer positions. (**c**) The efficiency of Mo ATG was verified through fluorescence extinction of co-injected *cdc20b-Venus*. (**d**) RT-PCR confirmed that Mo Spl caused intron1 retention (amplicon=191bp; double green stars), which is expected to introduce a premature stop codon and to produce a Cdc20b protein lacking 96% of its amino-acids, likely to undergo unfolded protein response-mediated degradation. (**e**) Immunostaining with the anti-*Xenopus* CDC20B antibody confirmed that both Mo ATG and Mo Spl severely down-regulated CDC20B protein expression in st18 MCCs. (**f**) RTqPCR revealed that neither *cdc20b* mopholinos caused significant *p53* transcript up-regulation, a non-specific response sometimes detected in zebrafish embryos subjected to morpholinos. Four independent experiments were carried out to check *p53* expression in morphant conditions. (**g**) miR-449 expression revealed by whole-mount *in situ* hybridization with LNA probes was not perturbed in the presence of either mopholinos. Embryos were photographed before (top) and after (bottom) staining against co-injected GFP-CAAX to be able to detect miR-449 staining. The number of embryos showing normal miR-449 expression over the total number of embryos analyzed is indicated on the photographs. Scale bars: 500µm (**c**), 5µm (**e**), 500µm (**g**, whole embryo), 80µm (**g**, zoom).

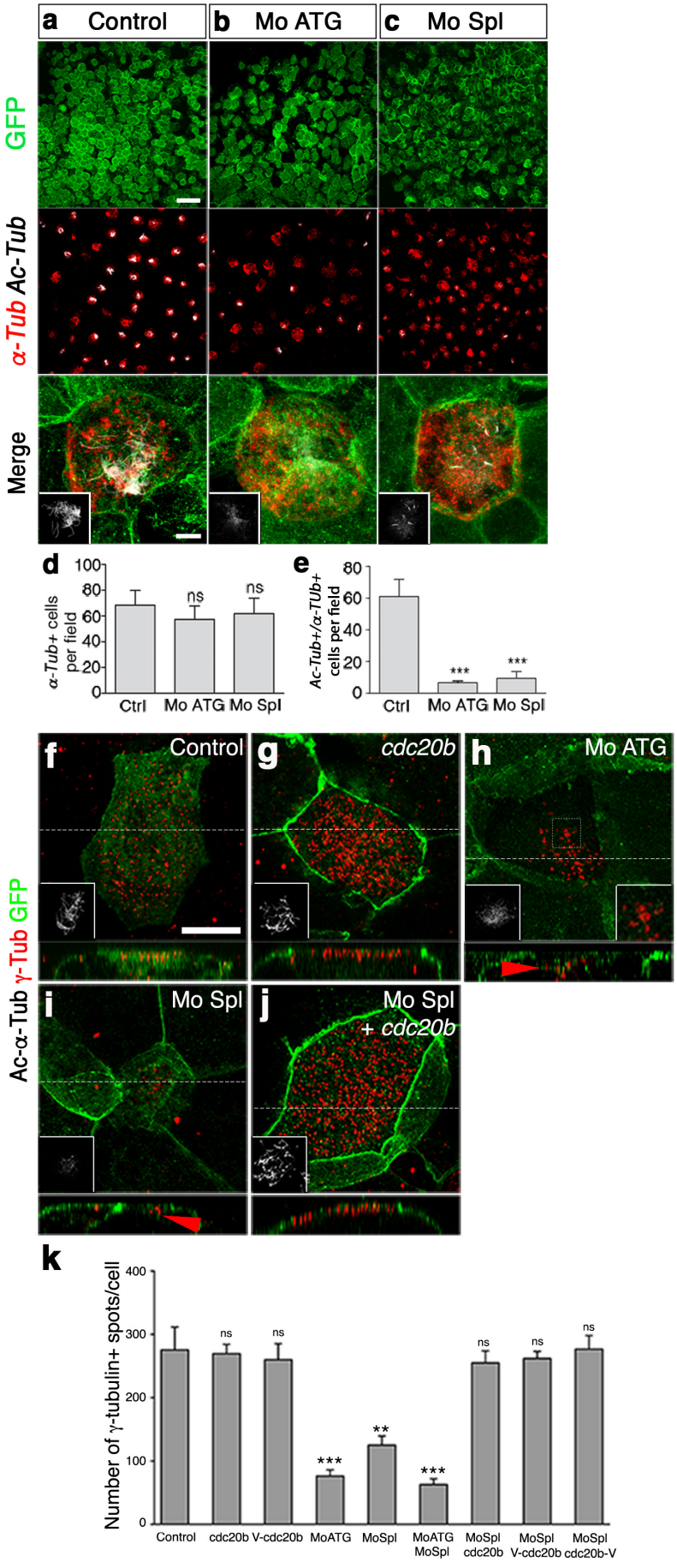

1131

Supplementary Figure 6: *cdc20b* knockdown impairs multiciliogenesis in *Xenopus*.

(**a**-**e**) 8-cell embryos were injected in presumptive epidermis with *cdc20b* morpholinos and *GFP-CAAX* mRNA (injection tracer) as indicated. Control was provided by *GPF-CAAX* injection alone. Embryos at tailbud st25 were processed for fluorescent staining against GFP (green), Acetylated α-Tubulin (cilia, white) and *α-Tub* mRNA (MCC marker, red). Insets on merged panels show cilia staining. Note that *cdc20b* morphant MCCs maintain expression of fate marker *α-Tub* but poorly grow cilia. (**d**) Bar graph showing quantification of *α-Tub*/GFP double positive cells per field of observation. (**e**) Bar graph showing quantification of *α-Tub*/Ac-Tub/GFP triple positive cells per field of observation. 10 fields corresponding to 10 different embryos were analyzed for each condition. (**f**-**k**) 8-cell embryos were injected in presumptive epidermis with *cdc20b* morpholinos, *GFP-CAAX* and *cdc20b* mRNAs as indicated, and immunostained at tailbud st25 against GFP (injection tracer, green), γ-tubulin (BBs, red) and Acetylated α-Tubulin (cilia, white, left insets). Right inset in **h**: zoom on a stalled deuterosomal figure. z-projections made along white dotted lines are shown in bottom panels. Arrowheads point undocked BBs. (**k**) Bar graph showing the quantification of γ-tubulin spots per MCC. As that two individual γ-tubulin spots are detected around each basal body, twice as many spots are usually counted as compared to Centrin (Fig. 5j-o). Note that BB numbers were restored to normal levels in *cdc20b* Spl morphants injected with tagged and untagged versions of *cdc20b*. Scale bars: 50µm (**a**, top), 5µm (**a**, bottom), 5µm (**f**).

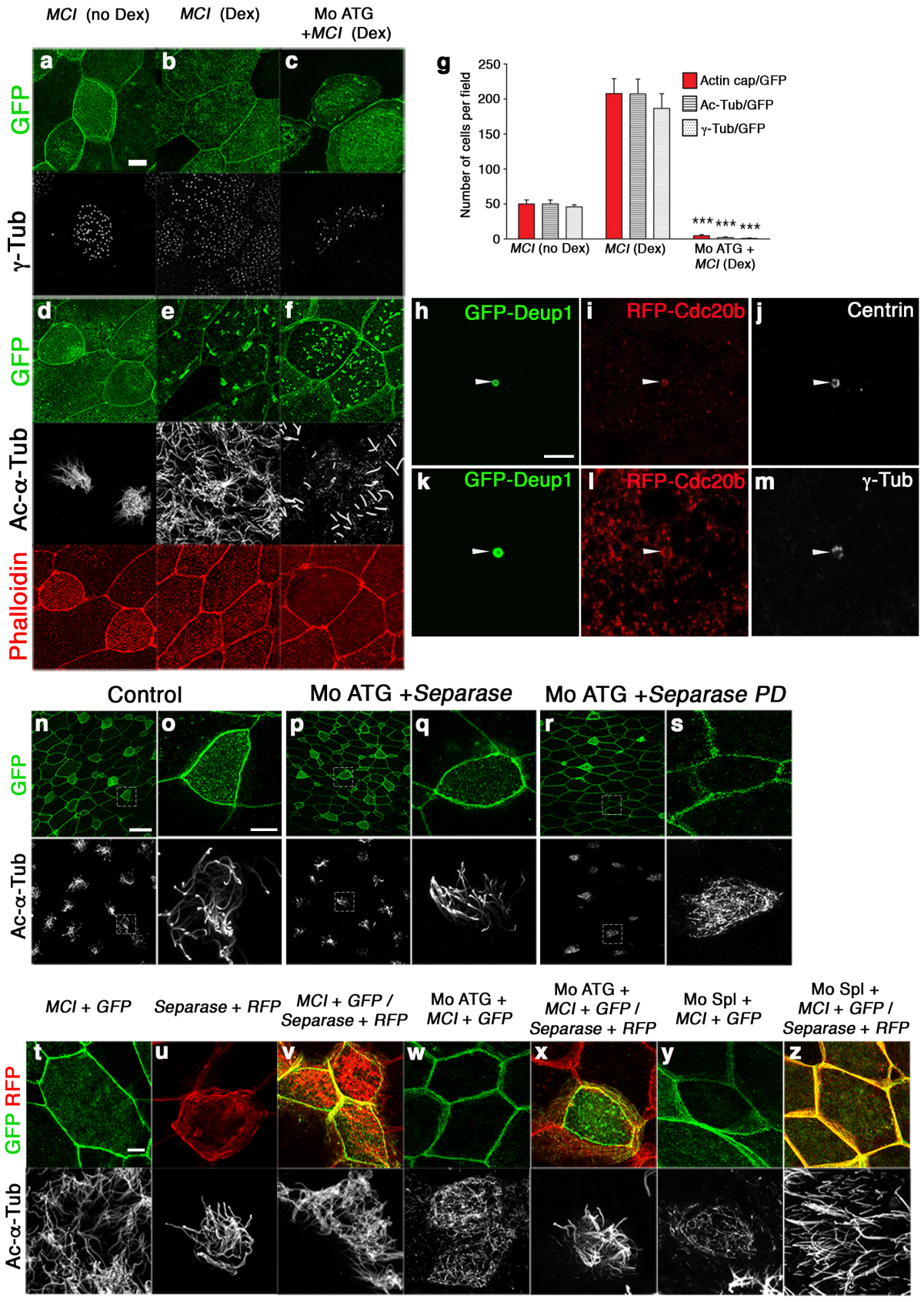

Supplementary Figure 7: *cdc20b* knockdown prevents multiciliogenesis induced by Multicilin, and is counteracted by Separase overexpression.

(**a**-**g**) ***cdc20b* knockdown prevents multiciliogenesis induced by Multicilin.** 8-cell embryos were injected in presumptive epidermis with *Multicilin-hGR* mRNA (*MCI*) and *cdc20b* Mo ATG, as indicated. *GFP-GPI* mRNA was co-injected as a tracer. MCI-hGR-injected embryos were induced with dexamethasone at st11. To check the efficiency of MCI induction some embryos were not treated with dexamethasone and served as controls (no DEX). Embryos were fixed at tailbud st25, and were stained against GFP (green) and γ-Tubulin (basal bodies, white)(**a**-**c**), or against GFP (green), phalloidin (apical actin, red), and Acetylated-α-Tubulin (cilia, white)(**d**-**f**). Note that *cdc20b* morphant MCI-induced MCCs failed to amplify centrioles, to maintain a proper actin cap, and to grow cilia. (**g**) Bar graph showing the quantification of GFP-positive cells that displayed normal actin, basal body and cilium staining. 5 fields (40x) per condition were analyzed. (**h**-**m**) **Deup1 recruits CDC20B in centriole amplification platforms.** 8-cell embryos were injected in presumptive epidermis with *Multicilin-hGR*, *RFP-CDC20B*, and *GFP-Deup1*mRNAs. Multicilin activity was induced with dexamethasone at st11, embryos were fixed at st18 and stained for GFP, RFP, Centrin (centrioles) or γ-Tubulin (deuterosome). White arrowheads point at active deuterosome-like structures formed around overexpressed GFP-Deup1, which incorporate RFP-CDC20B, consistent with their capacity to form a complex (Fig. 6c). (**n**-**z**) **Wild-type but not protease-dead Separase rescues multiciliogenesis in MCCs deficient for Cdc20b.** (**n**-**s**) 8-cell embryos were injected in presumptive epidermis with *GFP-GPI* mRNA, human *Separase* mRNA, and *cdc20b* Mo ATG, as indicated. Immunofluorescence against GFP (injection tracer, green), and Acetylated-α-Tubulin (cilia, white) was performed at tailbud st25. Cells in dotted squares were blown up for better visualization. Note that multiciliogenesis was rescued in *cdc20b* morphant MCCs by wild-type (**p**,**q**) but not protease-dead Separase (**r**,**s**). (**t**-**z**) 4-cell embryos were injected in one ventral blastomere (presumptive epidermis) with *MCI-hGR* and *GFP-GPI* mRNAs, in the presence or not of *cdc20b* morpholinos, as indicated. Next, at 16-cell stage, half of those

1180 embryos were injected with human *Separase* and RFP mRNAs in one ventral-animal
1181 blastomere. This setup was designed to avoid co-injection of *cdc20b* morpholinos with
1182 *Separase* mRNA, ruling out non-specific interference *in vitro* between these reagents. MCI-
1183 hGR-injected embryos were induced with dexamethasone at st11. All embryos were fixed at
1184 tailbud st25 and stained for GFP (*cdc20b* Mo tracer, green), RFP (*Separase* tracer, red) and
1185 Acetylated-α-Tubulin (cilia, white). Note that multiciliogenesis failed in MCI-induced *cdc20b*
1186 morphant MCCs (**w**,**y).** The presence of Separase rescued multiciliogenesis in MCI-induced
1187 *cdc20b* morphant MCCs (**x**,**z**). Scale bars: 5µm (**a**, **h**, **o**, **t**), 20µm (**n**).
1188

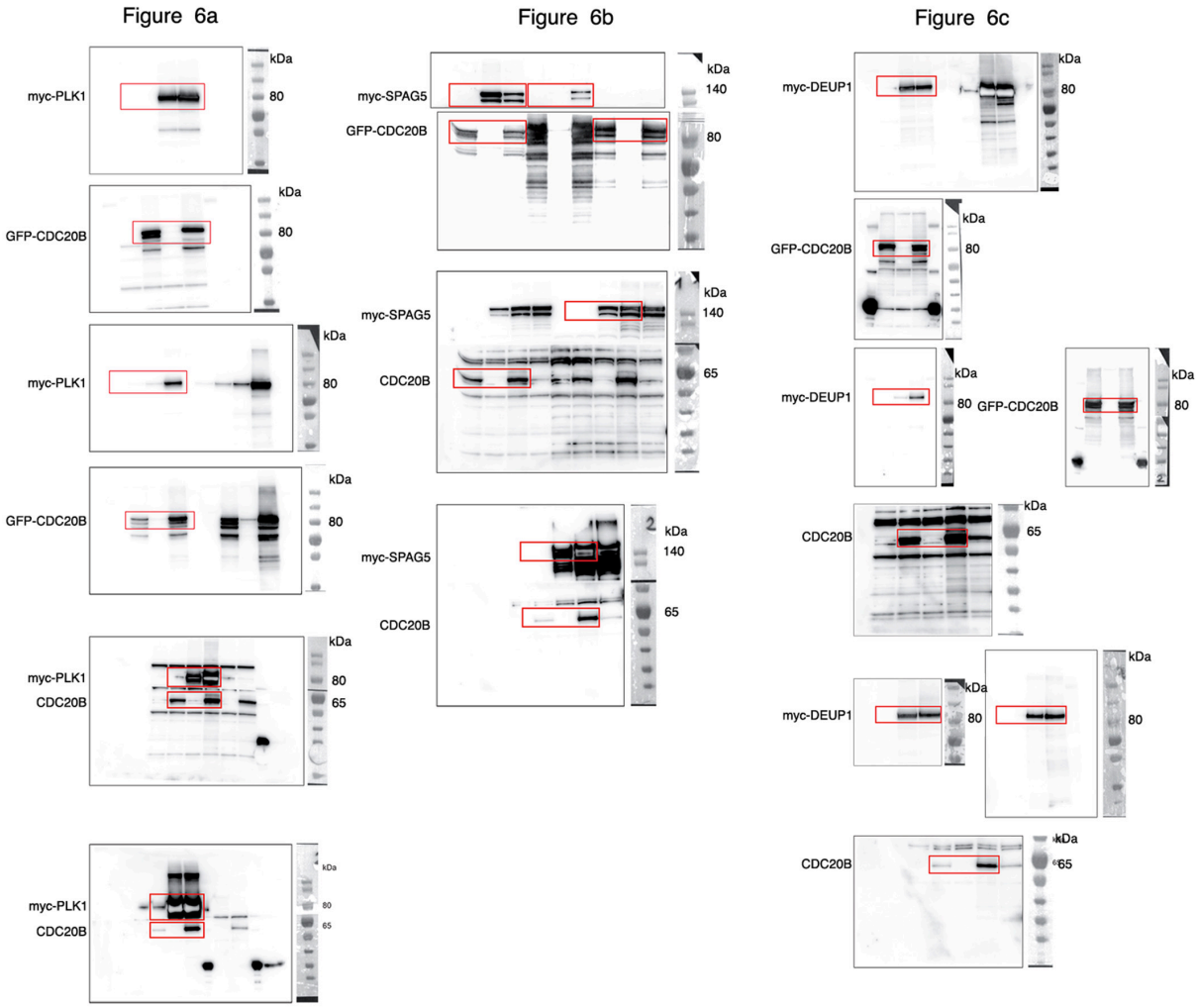

Supplementary Figure 8: Uncropped Western blots.

Red boxes mark the parts of the Western blot images that are shown in the indicated parts of Figure 6.

G1/S		S		G2/M		M		M/G1	
Symbol	Ensembl	Symbol	Ensembl	Symbol	Ensembl	Symbol	Ensembl	Symbol	Ensembl
ORC1	ENSG00000085840	ANKRD18A	ENSG00000273170	IQGAP3	ENSG00000183856	CKS1B	ENSG00000268942	TROAP	ENSG00000135451
ZNF367	ENSG00000165244	REEP1	ENSG00000068615	TRAIP	ENSG00000183763	DEPDC1B	ENSG00000035499	CDKN3	ENSG00000100526
ADAMTS1	ENSG00000154734	DEPDC7	ENSG00000121690	CDC25C	ENSG00000158402	SHCBP1	ENSG00000171241	PRC1	ENSG00000198901
CCNE2	ENSG00000175305	CDC7	ENSG00000097046	NEIL3	ENSG00000109674	FAM64A	ENSG00000129195	HSD17B11	ENSG00000198189
CDC25A	ENSG00000164045	DNA2	ENSG00000138346	PIF1	ENSG00000140451	FYN	ENSG00000010810	BTBD3	ENSG00000132640
RECQL4	ENSG00000160957	EXO1	ENSG00000174371	KIFC1	ENSG00000237649	KIF2C	ENSG00000142945	SLC39A10	ENSG00000196950
DTL	ENSG00000143476	KDELC1	ENSG00000134901	HJURP	ENSG00000123485	SPAG5	ENSG00000076382	GTF3C4	ENSG00000125484
CDC6	ENSG00000094804	ANKRD18A	ENSG00000180071	NCAPH	ENSG00000121152	CIT	ENSG00000122966	WWC1	ENSG00000113645
CCNE1	ENSG00000105173	BRIP1	ENSG00000136492	KIF23	ENSG00000137807	CENPA	ENSG00000115163	ELP3	ENSG00000134014
MCM2	ENSG00000073111	PKMYT1	ENSG00000127564	SKA3	ENSG00000165480	DIAPH3	ENSG00000139734	FOXK2	ENSG00000141568
GINS3	ENSG00000181938	CDC45	ENSG00000093009	KIAA1524	ENSG00000163507	CADM1	ENSG00000182985	OPN3	ENSG00000054277
CHAF1B	ENSG00000159259	C11orf82	ENSG00000165490	NDC80	ENSG00000080986	KIF14	ENSG00000118193	KIAA0586	ENSG00000100578
WDR76	ENSG00000092470	BLM	ENSG00000197299	CCNF	ENSG00000162063	PLK1	ENSG00000166851	ANTXR1	ENSG00000169604
MCM6	ENSG00000076003	RAD51	ENSG00000051180	CDCA8	ENSG00000134690	MDC1	ENSG00000137337	CEP70	ENSG00000114107
CLSPN	ENSG00000092853	CCDC150	ENSG00000144395	PSRC1	ENSG00000134222	DEPDC1	ENSG00000024526	HMGCR	ENSG00000113161
CDCA7	ENSG00000144354	CDCA5	ENSG00000146670	FANCD2	ENSG00000144554	BUB1	ENSG00000169679	TULP4	ENSG00000130338
OSBPL6	ENSG00000079156	CPNE8	ENSG00000139117	ESPL1	ENSG00000135476	DLGAP5	ENSG00000126787	ZNF281	ENSG00000162702
RAB23	ENSG00000112210	MCM8	ENSG00000125885	CDR2	ENSG00000140743	NUF2	ENSG00000143228	CDK7	ENSG00000134058
PLCXD1	ENSG00000182378	ESCO2	ENSG00000171320	AURKB	ENSG00000178999	CEP55	ENSG00000138180	LYAR	ENSG00000145220
SKP2	ENSG00000145604	GOLGA8B	ENSG00000215252	BORA	ENSG00000136122	GTSE1	ENSG00000075218	PPP6R3	ENSG00000110075
MDM1	ENSG00000111554	ASF1B	ENSG00000105011	LMNB1	ENSG00000113368	HMMR	ENSG00000072571	DCP1A	ENSG00000162290
GINS2	ENSG00000131153	FANCA	ENSG00000187741	TRIM59	ENSG00000213186	FOXM1	ENSG00000111206	FAM189B	ENSG00000160767
E2F1	ENSG00000101412	INTS7	ENSG00000143493	CHEK2	ENSG00000183765	E2F5	ENSG00000133740	AGPAT3	ENSG00000160216
MCM5	ENSG00000100297	POLA1	ENSG00000101868	MND1	ENSG00000121211	PRR11	ENSG00000068489	PSEN1	ENSG00000080815
SNHG10	ENSG00000247092	FANCI	ENSG00000140525	CDCA2	ENSG00000184661	NEK2	ENSG00000117650	NUP37	ENSG00000075188
HSF2	ENSG00000025156	RRM2	ENSG00000171848	CKAP2L	ENSG00000169607	TACC3	ENSG00000013810	MSL1	ENSG00000188895
UBR7	ENSG00000012963	TTLL7	ENSG00000137941	STIL	ENSG00000123473	CENPE	ENSG00000138778	AGFG1	ENSG00000173744
RMI2	ENSG00000175643	RAD51AP1	ENSG00000111247	POLQ	ENSG00000051341	CCNB2	ENSG00000157456	SNUPN	ENSG00000169371
NUP43	ENSG00000120253	KAT2B	ENSG00000114166	MELK	ENSG00000165304	CDC20	ENSG00000117399	STAG1	ENSG00000118007
ACD	ENSG00000102977	CHML	ENSG00000203668	CENPL	ENSG00000120334	BIRC5	ENSG00000089685	LRIF1	ENSG00000121931
ZMYND19	ENSG00000165724	BRCA1	ENSG00000012048	LIX1L	ENSG00000152022	CCDC88A	ENSG00000115355	PAK1IP1	ENSG00000111845
MSH2	ENSG00000095002	ABHD10	ENSG00000144827	KIF11	ENSG00000138160	POC1A	ENSG00000164087	NCOA3	ENSG00000124151
CDCA7L	ENSG00000164649	TYMS	ENSG00000176890	C14orf80	ENSG00000185347	MKI67	ENSG00000148773	PTTG1	ENSG00000164611
KIAA1586	ENSG00000168116	PRIM1	ENSG00000198056	UBE2C	ENSG00000175063	MKI67	ENSG00000148773	CTR9	ENSG00000198730
PMS1	ENSG00000064933	TTC31	ENSG00000115282	NCAPD3	ENSG00000151503	HSPA13	ENSG00000155304	DKC1	ENSG00000130826
UNG	ENSG00000076248	E2F8	ENSG00000129173	HAUS8	ENSG00000131351	CDC25B	ENSG00000101224	FOPNL	ENSG00000133393
KIAA1147	ENSG00000257093	CENPQ	ENSG00000031691	FAM83D	ENSG00000101447	TPX2	ENSG00000088325	VCL	ENSG00000035403
POLD3	ENSG00000077514	PHTF1	ENSG00000116793	CDK1	ENSG00000170312	AURKA	ENSG00000087586	MRPS2	ENSG00000122140
ANKRD10	ENSG00000088448	MASTL	ENSG00000120539	MAD2L1	ENSG00000164109	ANKRD40	ENSG00000154945	WIPF2	ENSG00000171475
CHAF1A	ENSG00000167670	OSGIN2	ENSG00000164823	GABPB1	ENSG00000104064	CENPF	ENSG00000117724		
BARD1	ENSG00000138376	GOLGA8A	ENSG00000175265	SAP30	ENSG00000164105	CNTROB	ENSG00000170037		
INTS8	ENSG00000164941	PHTF2	ENSG00000006576	CFD	ENSG00000197766	NCAPD2	ENSG00000010292		
APEX2	ENSG00000169188	BBS2	ENSG00000125124	TTF2	ENSG00000116830	SGOL2	ENSG00000163535		
ACYP1	ENSG00000119640	BMI1	ENSG00000168283	MID1	ENSG00000101871	SRF	ENSG00000112658		
MRI1	ENSG00000037757	FEN1	ENSG00000168496	GAS1	ENSG00000180447	DZIP3	ENSG00000198919		
INSR	ENSG00000171105	RMI1	ENSG00000178966	TUBA1A	ENSG00000167552	ECT2	ENSG00000114346		
TOPBP1	ENSG00000163781	NSUN3	ENSG00000178694	ZNF587	ENSG00000198466	ORAOV1	ENSG00000149716		
FAM105B	ENSG00000154124	KAT2A	ENSG00000108773	TUBD1	ENSG00000108423	NUP35	ENSG00000163002		
NPAT	ENSG00000149308	CENPM	ENSG00000100162	FAN1	ENSG00000198690	PTPN9	ENSG00000169410		
PCDH7	ENSG00000169851	ZWINT	ENSG00000122952	CDKN2C	ENSG00000123080	HS2ST1	ENSG00000153936		
GMNN	ENSG00000112312	ORC3	ENSG00000135336	TUBB2A	ENSG00000137267	RCAN1	ENSG00000159200		
RNPC3	ENSG00000185946	KIAA1598	ENSG00000187164	TNPO2	ENSG00000105576	SS18	ENSG00000141380		
RNF113A	ENSG00000125352	BIVM	ENSG00000134897	ZNHIT2	ENSG00000174276	HCFC1	ENSG00000172534		
FAM122A	ENSG00000187866	DNAJB4	ENSG00000162616	TRMT2A	ENSG00000099899	NUP98	ENSG00000110713		
CAPN7	ENSG00000131375	CCDC84	ENSG00000186166	PKNOX1	ENSG00000160199	POM121	ENSG00000196313		
TIPIN	ENSG00000075131	DCAF16	ENSG00000163257	ENTPD5	ENSG00000187097	TOMM34	ENSG00000025772		
C14orf142	ENSG00000170270	NUP160	ENSG00000030066	KDM4A	ENSG00000066135	CKAP5	ENSG00000175216		
LNPEP	ENSG00000113441	RFC2	ENSG00000049541	STK17B	ENSG00000081320	GRK6	ENSG00000198055		
USP53	ENSG00000145390	CDKN2AIP	ENSG00000168564	KLF6	ENSG00000067082	SEPHS1	ENSG00000086475		
PANK2	ENSG00000125779	UBE2T	ENSG00000077152	KATNA1	ENSG00000186625	QRICH1	ENSG00000198218		
VPS72	ENSG00000163159	DHFR	ENSG00000228716	H2AFX	ENSG00000188486	AHI1	ENSG00000135541		
DIS3	ENSG00000083520	PTAR1	ENSG00000188647	BRD8	ENSG00000112983	CNOT10	ENSG00000182973		
		RAD18	ENSG00000070950	RCCD1	ENSG00000166965	KLF9	ENSG00000119138		
		OGT	ENSG00000147162	CDKN1B	ENSG00000111276	SETD8	ENSG00000183955		
		EZH2	ENSG00000106462	UACA	ENSG00000137831	ATF7IP	ENSG00000171681		
		C5orf42	ENSG00000197603	KCTD9	ENSG00000104756	RAD51C	ENSG00000108384		
		LYRM7	ENSG00000186687	ATL2	ENSG00000119787	CDC42EP1	ENSG00000128283		
		CCDC14	ENSG00000175455	KPNA2	ENSG00000182481	HPS4	ENSG00000100099		
		NAB1	ENSG00000138386	HRSP12	ENSG00000132541	GOT1	ENSG00000120053		
		SP1	ENSG00000185591	VTA1	ENSG00000009844	MZT1	ENSG00000204899		
		RPA2	ENSG00000117748	HMGB2	ENSG00000164104	RRP1	ENSG00000160214		
		RBBP8	ENSG00000101773	C2orf69	ENSG00000178074	AKIRIN2	ENSG00000135334		
		RRM1	ENSG00000167325	FADD	ENSG00000168040	CDC27	ENSG00000004897		
		FAM178A	ENSG00000119906	HIPK2	ENSG00000064393	SMARCD1	ENSG00000066117		
		SAP30BP	ENSG00000161526	KIF22	ENSG00000079616	BIRC2	ENSG00000110330		
		NT5DC1	ENSG00000178425	MGAT2	ENSG00000168282				
		CERS6	ENSG00000172292	NR3C1	ENSG00000113580				
		ZBED5	ENSG00000236287	DHX8	ENSG00000067596				
		MAP3K2	ENSG00000169967	NMB	ENSG00000197696				
				TFAP2A	ENSG00000137203				
				HINT3	ENSG00000111911				
				CDC16	ENSG00000130177				
				NUMA1	ENSG00000137497				
				ARMC1	ENSG00000104442				
				STAT1	ENSG00000115415				
				CCDC107	ENSG00000159884				
				TMPO	ENSG00000120802				

Supplementary Table 1: Gene sets used to assess enrichment of cell cycle phases related transcripts in individual cells analyzed by scRNA-seq.

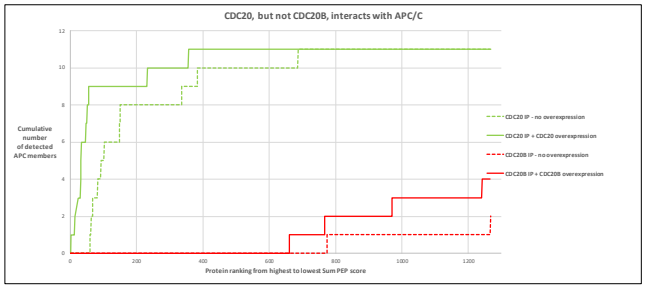

Protein ranking from highest to lowest Sum PEP score	Cumulative number of detected APC/C members			
	CDC20 IP - no overexpression	CDC20 IP + CDC20 overexpression	CDC20B IP - no overexpression	CDC20B IP + CDC20B overexpression
1	0	0	0	0
2	0	1	0	0
6	0	1	0	0
7	0	1	0	0
12	0	1	0	0
13	0	2	0	0
24	0	3	0	0
27	0	3	0	0
28	0	3	0	0
30	0	3	0	0
31	0	4	0	0
32	0	5	0	0
33	0	6	0	0
46	0	6	0	0
47	0	7	0	0
50	0	7	0	0
51	0	8	0	0
55	0	8	0	0
56	0	9	0	0
59	0	9	0	0
60	1	9	0	0
62	1	9	0	0
63	2	9	0	0
67	2	9	0	0
68	3	9	0	0
81	3	9	0	0
82	4	9	0	0
91	4	9	0	0
92	5	9	0	0
101	5	9	0	0
102	6	9	0	0
147	6	9	0	0
148	7	9	0	0
149	7	9	0	0
150	8	9	0	0
231	8	9	0	0
232	8	10	0	0
335	8	10	0	0
336	9	10	0	0
356	9	10	0	0
357	9	11	0	0
382	9	11	0	0
383	10	11	0	0
660	10	11	0	0
661	10	11	0	1
685	10	11	0	1
686	11	11	0	1
767	11	11	0	1
768	11	11	0	2
773	11	11	0	2
774	11	11	1	2
970	11	11	1	2
971	11	11	1	3
1241	11	11	1	3
1242	11	11	1	4
1265	11	11	1	4
1266	11	11	2	4

IP CDC20 - no overexpression

Protein FDR Confidence	Accession	Symbol	Description	Sum PEP Score	Coverage	# Peptides	# PSMs	# Unique Peptides	MW [kDa]	emPAI	Score Sequest HT	global rank	APC rank
High	Q9UJX2	CDC23	Cell division c	109,78	47,74	27	48	27	68,79	6,80	88,85	60	1,00
High	**Q12834**	**CDC20**	**Cell division c**	**104,51**	**49,70**	**16**	**56**	**16**	**54,69**	**10,94**	**158,30**	63	2,00
High	Q9H1A4	ANAPC1	Anaphase-pro	101,92	23,66	32	42	32	216,36	1,30	36,79	68	3,00
High	Q9UJX4	ANAPC5	Anaphase-pro	91,89	42,38	23	50	23	85,02	3,19	83,00	82	4,00
High	Q9UJX3;A0A024RBJ3	ANAPC7	Anaphase-pro	85,18	46,58	21	38	21	66,81	6,13	61,05	92	5,00
High	A0A024RD22;Q13042	CDC16	CDC16 cell div	79,32	43,55	21	31	21	71,61	4,37	48,14	102	6,00
High	P30260	CDC27	Cell division c	63,63	26,33	16	31	1	91,81	2,00	41,46	148	7,00
High	G5EA36	CDC27	Cell division c	63,28	26,25	16	31	1	91,68	2,00	41,49	150	8,00
High	Q9UJX6	ANAPC2	Anaphase-pro	37,09	22,75	13	15	13	93,77	0,93	15,24	336	9,00
High	Q9UJX5	ANAPC4	Anaphase-pro	31,69	16,34	13	13	13	92,06	0,89	7,67	383	10,00
High	Q9UM13	ANAPC10	Anaphase-pro	16,01	31,89	5	9	5	21,24	1,85	11,56	686	11,00

IP CDC20 + CDC20 overexpression

Protein FDR Confidence	Accession	Symbol	Description	Sum PEP Score	Coverage	# Peptides	# PSMs	# Unique Peptides	MW [kDa]	emPAI	Score Sequest HT	global rank	APC rank
High	Q9H1A4	ANAPC1	Anaphase-pro	710,46	59,57	81	319	81	216,36	28,94	640,59	2	1
High	Q9UJX4	ANAPC5	Anaphase-pro	463,89	66,23	50	288	46	85,02	142,07	635,28	13	2
High	Q9UJX5	ANAPC4	Anaphase-pro	371,59	59,53	43	198	43	92,06	34,74	384,67	24	3
High	**Q12834**	**CDC20**	**Cell division c**	**332,93**	**69,54**	**28**	**791**	**28**	**54,69**	**202,09**	**1712,61**	28	3
High	P30260	CDC27	Cell division c	306,64	60,56	34	215	1	91,81	20,92	435,97	31	4
High	G5EA36	CDC27	Cell division c	306,44	60,51	34	212	1	91,68	20,92	426,79	32	5
High	Q9UJX6	ANAPC2	Anaphase-pro	301,10	54,50	45	165	45	93,77	27,12	297,57	33	6
High	A0A024RD22;Q13042	CDC16	CDC16 cell div	253,91	55,00	29	108	29	71,61	22,90	226,42	47	7
High	Q9UJX2	CDC23	Cell division c	244,49	54,77	33	121	33	68,79	27,80	262,31	51	8
High	Q9UJX3;A0A024RBJ3	ANAPC7	Anaphase-pro	236,24	64,61	32	117	32	66,81	37,75	239,65	56	9
High	Q9UM13	ANAPC10	Anaphase-pro	86,65	76,22	11	43	11	21,24	27,48	98,76	232	10
High	I3L3H6	CDC27	Cell division c	63,60	63,09	7	32	1	25,91	5,81	75,14	357	11

IP CDC20 B-no overexpression

Protein FDR Confidence	Accession	Symbol	Description	Sum PEP Score	Coverage	# Peptides	# PSMs	# Unique Peptides	MW [kDa]	emPAI	Score Sequest HT	global rank	APC rank
High	Q9UJX5	ANAPC4	Anaphase-pro	7,09	3,47	1	2	1	92,06	0,05	2,13	774	1
High	A0A024RD22;Q13042	CDC16	CDC16 cell div	2,31	4,68	1	1	1	71,61	0,06	0,00	1266	2

IP CDC20 B + CDC20B overexpression

Protein FDR Confidence	Accession	Symbol	Description	Sum PEP Score	Coverage	# Peptides	# PSMs	# Unique Peptides	MW [kDa]	emPAI	Score Sequest HT	global rank	APC rank
High	**Q86Y33**	**CDC20B**	**Cell division c**	**215,12**	**60,89**	**26**	**271**	**26**	**57,30**	**41,99**	**546,93**	7	0
High	Q9UJX2	CDC23	Cell division c	11,98	12,90	5	5	5	68,79	0,37	0,00	661	1
High	A0A024RD22;Q13042	CDC16	CDC16 cell div	9,77	5,65	3	3	3	71,61	0,21	3,53	768	2
High	P30260	CDC27	Cell division c	6,89	3,64	3	3	3	91,81	0,17	3,63	971	3
High	Q9UJX3;A0A024RBJ3	ANAPC7	Anaphase-pro	4,21	6,18	2	2	2	66,81	0,15	0,00	1242	4

Supplementary Table 2: CDC20, but not CDC20B, interacts with APC/C.